JGR Biogeosciences

RESEARCH ARTICLE
10.1029/2025JG009415

Special Collection:
Changing biogeochemical cycles along the land-to-ocean aquatic continuum

Aquatic Productivity Signals in the Kolyma River (Northeastern Siberia) From O_2/Ar Ratios and O_2 Triple Isotopologues

K. Castro-Morales[1], A. Canning[2], S. Arzberger[1], J. Kaiser[3], W. A. Overholt[1], A. Sellmaier[1], N. Khodabakhshi[1], S. Redlich[4], A. Marca[3], O. Kolle[5], M. Göckede[5], T. Wichard[4], K. Küsel[1,6], A. Körtzinger[2,7], and N. Zimov[8]

[1]Friedrich Schiller University Jena, Institute of Biodiversity, Jena, Germany, [2]GEOMAR Helmholtz Centre for Ocean Research Kiel, Kiel, Germany, [3]University of East Anglia, School of Environmental Sciences, Centre for Ocean and Atmospheric Sciences, Norwich, UK, [4]Friedrich Schiller University Jena, Institute for Inorganic and Analytical Chemistry, Jena, Germany, [5]Max Planck Institute for Biogeochemistry, Jena, Germany, [6]German Centre for Integrative Biodiversity Research (iDiv) Halle-Jena-Leipzig, Leipzig, Germany, [7]Christian Albrecht University Kiel, Kiel, Germany, [8]North-East Science Station, Pacific Institute for Geography, Far-Eastern Branch of Russian Academy of Sciences, Chersky, Russia

Abstract Arctic rivers are intricate water networks that chemically and biologically process carbon before releasing it as carbon dioxide (CO_2) into the atmosphere or carrying it to the ocean. Primary producers use inorganic carbon to build biomass at the base of the trophic chain. Little is known about how biogeochemical properties in Arctic rivers adapt to climate warming and changes in hydrology. To quantify net and gross biological productivity, we measured the dissolved oxygen-to-argon (O_2/Ar) ratios and O_2 triple isotopologues composition in the river Kolyma and in its tributary Ambolikha during late freshet (June) and low-flow conditions (August) in 2019. We found that hydrological factors restricted river productivity. The river system released CO_2 into the atmosphere in June and August, however August emissions were only 6% of late freshet emissions. In June, higher river flow and turbidity restricted river production, but in August, lower flows allowed more light penetration and a phytoplankton bloom at the tributary-main Kolyma channel confluence. CO_2 emissions per area during June and August accounted for 5 ± 11% of the gross carbon uptake estimated during a bloom event. Thus, in-stream metabolism can exceed riverine CO_2 emissions under certain flow and light conditions. Arctic climate change may promote biological productivity in particular locations along with changes in dissolved organic matter signature and microbiome, and contribute to Arctic river carbon budgets as flow slows during prolongued open water periods.

Plain Language Summary Arctic rivers are complex systems of water that break down carbon chemically and biologically before releasing it into the air as carbon dioxide (CO_2) or taking it to the ocean. Tiny organisms at the base of the food chain, called primary producers, use CO_2 to create their food and build up their bodies with the support of light and nutrients. However, we do not fully understand how they adjust to climate change in the Arctic. In 2019, we measured the concentration of oxygen and argon and identified the different sources of oxygen in the water to calculate the amount of carbon that is consumed and released in the Kolyma and Ambolikha rivers in northeastern Siberia. We found that in June, after the snow and ice melt period, the river mainly releases CO_2 to the atmosphere, and there are few primary producers because the river is turbid. However, as the river flow settles down in August, more light penetrates the water column, and in some river areas, primary producers grow. Extended ice-free periods and reduced flow in Arctic rivers favor the growth and establishment of primary producers.

Key Points:

- Kolyma and Ambolikha rivers are large CO_2 emitters in the late-freshet, but CO_2 emissions decrease considerably during the low-flow period
- High river flows and turbidity restrict river productivity during late-freshet in June
- Increased light penetration and nutrients allow phytoplankton blooms in river-stream confluences during low-flow conditions in August

Supporting Information:

Supporting Information may be found in the online version of this article.

Correspondence to:

K. Castro-Morales,
karel.castro.morales@uni-jena.de

Citation:

Castro-Morales, K., Canning, A., Arzberger, S., Kaiser, J., Overholt, W. A., Sellmaier, A., et al. (2025). Aquatic productivity signals in the Kolyma River (northeastern Siberia) from O_2/Ar ratios and O_2 triple isotopologues. *Journal of Geophysical Research: Biogeosciences*, *130*, e2025JG009415. https://doi.org/10.1029/2025JG009415

Received 11 SEP 2025
Accepted 13 NOV 2025

Author Contributions:

Conceptualization: K. Castro-Morales
Data curation: K. Castro-Morales, A. Canning, S. Arzberger, J. Kaiser, W. A. Overholt, A. Sellmaier, N. Khodabakhshi, S. Redlich, A. Marca, O. Kolle, M. Göckede, T. Wichard
Formal analysis: K. Castro-Morales, A. Canning, S. Arzberger, J. Kaiser, W. A. Overholt, A. Sellmaier,

1. Introduction

The Arctic has warmed four times faster than the global average over the past four decades (Meredith et al., 2019; Rantanen et al., 2022). This rapid warming is reshaping Arctic hydrology, with earlier melt, prolonged open-water seasons, and intensifying river discharge (Francis et al., 2023; Holmes et al., 2021b). Arctic rivers show extreme seasonality: high flows during the May-June snowmelt ("freshet") and low flows in late summer from August to October. Discharge in the eight largest Arctic rivers has varied since the 1930s, and recent increases are linked to greater winter snowfall (Holmes et al., 2021a). Permafrost thaw alters runoff patterns and discharge regimes by increasing groundwater contributions to rivers (Frey & McClelland, 2009), while thaw-driven erosion and

N. Khodabakhshi, S. Redlich, A. Marca, T. Wichard
Funding acquisition: K. Castro-Morales
Investigation: K. Castro-Morales, A. Canning, S. Arzberger, J. Kaiser, W. A. Overholt, A. Sellmaier, N. Khodabakhshi, S. Redlich, A. Marca, O. Kolle, M. Göckede, T. Wichard, K. Küsel, A. Körtzinger, N. Zimov
Methodology: K. Castro-Morales, A. Canning, J. Kaiser, W. A. Overholt, T. Wichard
Project administration: K. Castro-Morales
Resources: K. Castro-Morales, J. Kaiser, M. Göckede, T. Wichard, K. Küsel, A. Körtzinger, N. Zimov
Supervision: K. Castro-Morales
Visualization: K. Castro-Morales, W. A. Overholt, S. Redlich, T. Wichard
Writing – original draft: K. Castro-Morales, A. Canning, W. A. Overholt, S. Redlich, T. Wichard
Writing – review & editing: K. Castro-Morales, A. Canning, J. Kaiser, W. A. Overholt, S. Redlich, A. Marca, M. Göckede, T. Wichard, K. Küsel, A. Körtzinger, N. Zimov

thermokarst reshape channels, influence sediment dynamics, and modify habitat structure (Costard et al., 2007). These processes mobilize nutrients, ancient organic carbon, gases, metals and microbes from land to rivers (Barbato et al., 2022; Francis et al., 2023; O'Donnell et al., 2016, 2024; Schuur et al., 2015; Serikova et al., 2018) with the potential to transform river metabolism, biodiversity, and the balance between carbon sources and sinks (Vonk, Tank, Bowden, et al., 2015).

Arctic Rivers transport and transform allochthonous material and generate autochthonous carbon (Spencer et al., 2008; Vonk, Tank, Mann, et al., 2015), and are typically net carbon dioxide (CO_2) sources to the atmosphere (Dean et al., 2020; Raymond et al., 2013). In boreal streams, high light, shallow depths, and nutrient loads stimulate algal growth (Burrows et al., 2021), while variation in light and flow strongly controls gross primary production and respiration in rivers across the US (Bernhardt et al., 2022). Aquatic metabolic processes contribute significantly to CO_2 emissions and diel patterns, as evidenced from continuous CO_2 and O_2 measurements and $^{13}C/^{12}C$ isotope ratios of dissolved inorganic carbon (DIC) in streams of Sweden and Alaska (Rocher-Ros et al., 2019, 2020).

Permafrost-derived dissolved organic matter (P-DOM) is more labile than bulk river DOM (Bowen et al., 2020; Cory et al., 2014; Mann et al., 2012; Spencer et al., 2015; Stubbins et al., 2017). As permafrost carbon is released upon soil thaw, the subsequent photochemical and microbial decomposition of organic substances in the river, from both ancient (permafrost) and modern sources, adds to the CO_2 pool available for transfer and evasion (Dean et al., 2020; Hotchkiss et al., 2015; Mann et al., 2015; Schuur et al., 2015, 2022; Turetsky et al., 2020). CO_2 emissions are modulated by discharge, peaking during high-flow periods (Liu & Raymond, 2018). Arctic rivers in western Siberia emit roughly twice as much CO_2 to the atmosphere than the carbon exported laterally to the Arctic Ocean. Most riverine CO_2 emissions are derived from terrestrial carbon decomposed under warm temperatures and long water residence times (Serikova et al., 2018).

On an annual scale, Arctic river CO_2 emissions likely surpass CO_2 uptake by autotrophic organisms (Hotchkiss et al., 2015), yet the metabolic balance between aquatic productivity and respiration under climate change remains poorly constrained (Fritz et al., 2017; Hobbie et al., 1999; Meredith et al., 2019). High sunlight exposure during ice-free periods enhances photochemical terrestrial dissolved organic carbon (DOC) degradation in Arctic rivers (Cory et al., 2014). Human interventions, such as river damming, alter flow and substances and influence phytoplankton productivity (Engel et al., 2019). This has been observed at the Kolymskoe dammed area in the upper Kolyma in northeastern Siberia, where the local phytoplankton assemblages vary due to changes in the hydrological regime (Gabyshev & Gabysheva, 2013; McClelland et al., 2004). Combined sunlight exposure, permafrost thaw, and hydrological modifications shape ecosystem structure, biodiversity, carbon processing and river metabolism (Fritz et al., 2017; Hobbie et al., 1999; Meredith et al., 2019; Wrona et al., 2006).

Northern high latitude marine and lacustrine (lakes and ponds) productivity has been previously quantified (Bogard et al., 2017; Codispoti et al., 2013; Matrai et al., 2013; Squires et al., 2009), and its controlling mechanisms, such as the role of nutrients and freshwater influx, have been well studied (Ayala-Borda et al., 2024; Myrstener et al., 2022; Terhaar et al., 2021; Yun et al., 2016). Riverine productivity estimates in the Arctic are scarce and often indirect. In Kolyma River, aquatic productivity has been inferred from depletion of ^{13}C and ^{14}C in riverine organic matter (Bröder et al., 2020; Keskitalo et al., 2022; Wild et al., 2019), or via the quantification of phytoplankton biomass (Gabyshev & Gabysheva, 2013; Vishnivetskaya et al., 2020), also in the Lena River (Sorokin & Sorokin, 1996). This gap limits our ability to predict ecosystem responses to permafrost thaw and hydrological regulation.

Here we present the first direct measurements of O_2/Ar ratios and the triple isotopologue composition of dissolved O_2 to quantify net (N) and gross (G) O_2 productivity in the water column of rivers Kolyma and Ambolikha in northeastern Siberia. These techniques allow the accurate differentiation of biological and non-biological oxygen sources in natural waters. This study is the first application of these methods in Arctic rivers.

We complement these measurements with the characterization of riverine dissolved organic matter and microbial community assemblages. In Arctic rivers, the bioavailability of carbon strongly shapes microbial and phytoplankton productivity (Berggren et al., 2012). The availability of the labile P-DOM in rivers provides direct carbon sources for primary producers. Also, microbial assemblages mediate carbon availability to primary producers across the Arctic river network (Castro-Morales, Canning, Körtzinger, et al., 2022; Castro-Morales, Canning, Arzberger, et al., 2022; Crump et al., 2009; Vonk, Tank, Bowden, et al., 2015). Characterizing DOM

composition and microbial communities thus offers key insights into carbon sources, transformation, and ecosystem responses to permafrost thaw and climate change.

To better understand the environmental controls of productivity in Kolyma and Ambolikha rivers, we also measured the dissolved oxygen concentration ($c(O_2)$), the partial pressure of CO_2 ($p(CO_2)$) and a suite of other chemical and biological properties. We hypothesized that aquatic productivity in Arctic rivers is enhanced during the less turbid open-water period. Therefore, our measurements were done along transects of these rivers during June (late-freshet period) and August (low-flow period) of 2019 to provide a spatiotemporal perspective.

The integrated approach presented in this study provides new insights into the mechanisms driving aquatic metabolism in Arctic rivers and how these may shift under continued warming. This work complements previous studies from the same campaign that examined (a) the influence of flow variation on the temporal dynamics of biogeochemical properties in the Ambolikha River (Castro-Morales, Canning, Körtzinger, et al., 2022), and (b) the spatial distribution of dissolved methane in the Kolyma and Ambolikha rivers (Castro-Morales, Canning, Arzberger, et al., 2022).

Reference to those works is done throughout the manuscript to avoid repetition in methodologies. By combining DOM composition and microbial community structure within the same analytical framework, the present study builds upon earlier efforts to provide a more mechanistic understanding of riverine biogeochemical responses to environmental change.

2. Methods

We conducted fieldwork in 2019 in the permafrost-dominated Kolyma River (120 km transect) and its tributary Ambolikha (16 km transect) in northeastern Siberia, using a small research vessel equipped with continuous flow-through sensors and discrete sampling devices (2.1). Sampling covered the ice-free season, with three transects during late freshet (June) and two during low-flow conditions (August). At 25 (June) and 13 (August) stations, we collected continuous measurements (CO_2, O_2, pH, temperature, turbidity, DOM fluorescence, nutrients) and discrete samples (2.2). Our combined approach analyzed for gas fluxes using O_2/Ar ratios and isotopologues (2.3), gross oxygen productivity (2.4), DOM molecular signatures (2.5), and complementary microbial composition analysis (2.6). Together, these methods allowed us to link hydrology, biogeochemistry, and microbial dynamics across seasonal transitions.

2.1. Study Area

The Kolyma River system in northeastern Siberia has a watershed area of 6.53×10^5 km^2 that is completely underlain by continuous permafrost, being the sixth largest Arctic river basin (Holmes et al., 2012). We sampled a section of 120 km along the main channel of the Kolyma, bounded at the downstream eastern end by the city of Chersky (68°45′5.1″N, 161°18′16.6″E), and at the upstream western end by the Duvannyi Yar site (68°38′12.8″N, 159°5′25.4″E; Figure 1).

We also sampled a 16 km-transect of the Ambolikha (a third Strahler order tributary of the Kolyma) between its confluence with the Pantheleikha River (a direct tributary of the Kolyma) at the downstream northern end (161°24′47.019″N, 68°44′21.901″E) and the Ambolikha site at the upstream southern end (68°36′46.73″N, 161°21′9.54″E; Castro-Morales, Canning, Körtzinger, et al., 2022; Figure 1).

The freshet period in Arctic River basins is defined as the flooding period during the spring thaw that takes place every year between May and June (Mann et al., 2012). In 2019, the freshet in the Kolyma started on 20 May (0.84×10^3 m^3 s^{-1}) and ended on 10 July (3.09×10^3 m^3 s^{-1}), reaching its peak on 31 May (27.7×10^3 m^3 s^{-1}). Our sampling took place during the ice-free season between 20 May and 12 October 2019 (146 days). These dates were obtained from the steep inflexions in the hydrograph of the daily discharge (Figure S1 in Supporting Information S1) at Kolymsk-1 gauge station (68°43′48″N, 158°43′12″E) located 40 km upstream of station 25 (Figure 1). Continuous measurements and discrete water samples were collected at 25 stations during the late-freshet and at 13 stations during the low-flow period (Figure 1). We navigated the indicated river sections twice using a small vessel: (a) During the late freshet between 15 and 17 June 2019, Kolyma both upstream and downstream directions between Chersky and Duvannyi Yar, and on 18 June 2019, Ambolikha upstream (i.e., three transects during the late freshet). (b) During the low-flow period, on 5 August 2019, we navigated the Kolyma downstream from Duvannyi Yar to Chersky, and on 8 August 2019, we navigated the Ambolikha

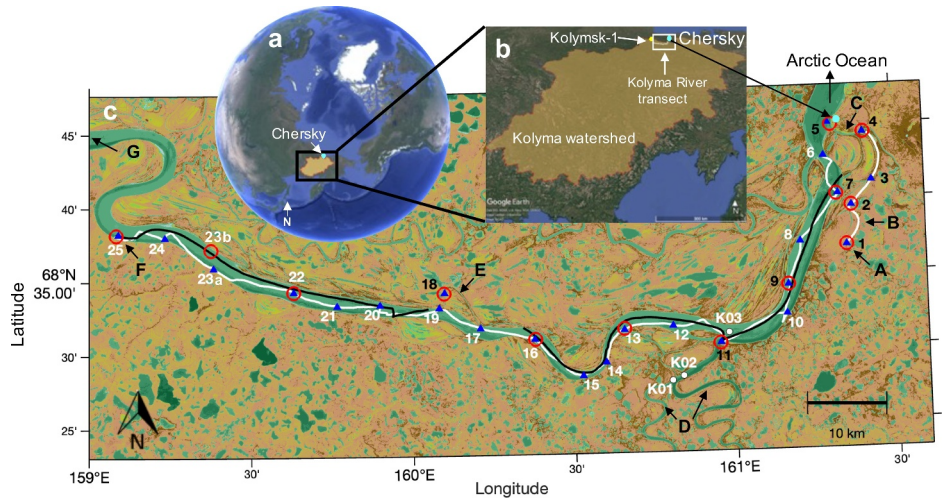

Figure 1. (a) Kolyma watershed extension (Makarieva et al., 2020), (b) Location of the navigated Kolyma and Ambolikha sections within the watershed, and the city of Chersky (cyan marker), (c) Navigated transects: white line, upstream direction Kolyma main channel (15–16 June 2019), and Ambolikha tributary (18 June 2019). Black line, downstream (17 June 2019). Blue triangles, 25 stations sampled in June. Red circles, 13 stations sampled in August. Letters indicate key sites: A—Ambolikha site at station 1, B—Ambolikha River, C—Pantheleika River, D—Rivers Malyi and Bolshoi Anui, E—Leonid's channel, F—Duvannyi Yar, and G—direction toward Omolon River and Kolymsk-1 station (yellow marker in panel b). Station numbers shown in black are inside or at the confluence of tributaries: stations 1–5, 7, 9, 11 and 18. Station 23a was sampled in June; station 23b in August.

upstream (i.e., two transects during the low-flow period). The measurements primarily occurred at the center of the channels, along riverbanks at the confluences of main tributaries, and in areas adjacent to floodplains where runoff from land with a high load of sediments and the presence of turbid water was observed.

2.2. Continuous and Discrete Measurements of Chemical Water Properties

Direct measurements of the partial pressure of CO_2, $p(CO_2)$, were only done in June. For this, a flow-through (FT) system was continuously fed with surface river water (intake 1 m below the water surface) pumped from the port side of the vessel. The water was delivered through PVC tubing branched into two outlets that fed the FT-system and a 20 L FT box containing an EXO2 multiparameter sonde (see below). Both flow paths had approximately the same flow rate (8.4 L min^{-1}). A SBE45 thermosalinograph (Sea-Bird Electronics, Bellevue, USA) was used to measure the temperature and salinity of the river water. The FT system was equipped with a membrane-based HydroC CO_2-FT sensor for non-dispersive infrared (NDIR) measurements (-4H-JENA engineering GmbH, Jena Germany). The sampling interval of the FT-CO_2 sensor was 5 s; its response time was approximately 1 min at 16°C under a flow rate of 5 L min^{-1} according to the manufacturer (Canning et al., 2021). The CO_2-FT sensor was calibrated prior to the measurement campaign by the manufacturer. Post-calibration and data validation after the campaign were done following Canning et al. (2021). Zeroing measurements (i.e., with all CO_2 stripped from the internal measurement gas circuit) were done at regular intervals through the measurement period for linear zero drift correction.

Because the FT-system was not used during the August sampling, $p(CO_2)$ measurements for this period were derived from total alkalinity (A_T) and pH measurements in discrete samples collected at stations along the river channels (Figure 1). Alkalinity samples were collected in acid-washed 250 mL amber glass flasks and kept in cold and dark conditions until their analysis <24 hr later. Samples were brought to room temperature and a 100 mL-aliquot was filtered through a 0.2 µm-membrane syringe filter. A_T was measured in the filtrate using potentiometric Gran-plot titration methods (DOE, 1994) in two replicates per sample. A_T had a precision of 16.7 µmol L^{-1} for replicate samples and 25 µmol L^{-1} for replicate standards, which is high due to the manual burette reading error of 5%. A_T was corrected for organic ions that is organic alkalinity (Abril et al., 2015), using the empirical equation of Oliver et al. (1983) based on measured pH and dissolved organic carbon concentration (c(DOC)), which gave an average contribution of 11 ± 7% organic alkalinity to A_T. This contribution is largest when c(DOC) is higher, for example, during the freshet, when it was 23 ± 9%. The CO2SYS program (Lewis et al., 1998) was

Table 1
Water Properties Along the Transects During the Late Freshet (June 2019)

		Kolyma 15–17 June 2019		Ambolikha 18 June 2019
Parameter	Unit	Upstream	Downstream	Upstream
T	°C	13.9 ± 0.5	14.5 ± 0.5	19.6 ± 0.3
κ	µS cm^{-1}	94 ± 21	107 ± 18	50 ± 1
pH	1	7.2 ± 0.1	7.2 ± 0.1	6.4 ± 0.2
fDOM concentration	QSU	55.6 ± 10.9	59.3 ± 4.9	99.7 ± 5.2
Turbidity	FNU	109 ± 102	34 ± 9	7 ± 2
c(Chl *a*)	µg L^{-1}	2.7 ± 0.5	2.4 ± 0.3	7.2 ± 0.7
c(blue-green algae)	µg L^{-1}	0.7 ± 0.4	0.3 ± 0.04	0.2 ± 0.01
c(TAlgae)	µg L^{-1}	3.4 ± 0.9	2.7 ± 0.4	7.5 ± 0.7
$c(O_2)$	mg L^{-1}	11.5 ± 0.2	11.4 ± 0.2	6.4 ± 0.2
$\Delta(O_2)$	%	11.0 ± 1.5	11.6 ± 0.9	−30.5 ± 1.5
$p(CO_2)$	µatm	1578 ± 281	1686 ± 266	5162 ± 530

Note. All parameters were statistically different at a 5% significance level (Wilcoxon rank-sum test) when compared between transects.

used to calculate $p(CO_2)$ from pH (EXO2 sonde; see below) and A_T corrected for organic alkalinity using freshwater dissociation constants from Millero (1979).

An EXO2 multiparameter sonde was immersed into the FT box for continuous measurements of water properties at a temporal resolution of 5 s: We measured water temperature (T, in °C), electrical conductivity (κ, in µS cm^{-1}), pH, dissolved oxygen concentration ($c(O_2)$, in mg L^{-1}), turbidity (in Formazin Nephelometric Units, FNU), fluorescent dissolved organic matter (fDOM) concentration (in Quinine Sulfate Units, QSU; equivalent to 1.28 µmol L^{-1} quinine sulfate dissolved in 0.105 mol L^{-1} perchloric acid), and the concentration of total algae c (TAlgae) with a dual optical channel for chlorophyll *a* (Chl *a*) and blue-green algae (BGA) concentration (both in µg L^{-1}; Table 1). T and $c(O_2)$ were corrected for an increase of 0.6°C and 1.2 mg L^{-1} (37.5 µmol L^{-1}) of $c(O_2)$, during travel through the PVC pipes. The continuous data streams were time-synchronized and averaged into 1-min bins to compensate for the different response times of the different measurements. In August, the EXO2 sonde was used to measure the same water properties as in June, but only for point measurements at 1 m below the water surface and selected vertical profiles (Figure 1). The EXO2 sensors were factory-calibrated before the field work. Two-point calibration standard checks were carried out for $c(O_2)$ and pH on-site before and after the measurements to evaluate sensor drift, which was not observed. fDOM concentrations are reported at a reference temperature of 25°C (Downing et al., 2012; Watras et al., 2011) and corrected for the influence of turbidity on light attenuation following Snyder et al. (2018).

2.2.1. Discrete Water Sampling for Ancillary Water Analytes

Discrete water samples were collected at 25 sites during June late-freshet and at 13 stations during the August low-flow period. Except for station 23, the same location were occupied at both times (Figure 1). The water was collected from 1 m below the water surface with a 1.5 L Niskin bottle and divided into six aliquots using silicone tubing (Supplement A in Supporting Information S1) in the following order: (a) O_2/Ar ratios and O_2 triple isotopologues (Sections 2.3 and 2.4), (b) DOC concentration (c(DOC); in mmol L^{-1}), and A_T for the August samples; Section 2.2), (c) nutrient concentrations $c(SiO_3^{2-})$, $c(PO_4^{3-})$, and $c(NO_x^-) = c(NO_3^-) + c(NO_2^-)$; all in µmol L^{-1}; Table S1 in Supporting Information S1), (d) characterization of DOM by high-resolution mass-spectrometry (Section 2.5; Supplement B in Supporting Information S1), (e) hydrogen and oxygen stable isotope composition of water, $\delta(^2H, H_2O)$ and $\delta(^{18}O, H_2O)$, relative to Vienna Standard Mean Ocean Water (VSMOW), and (f) microbial community composition (Section 2.6; Supplement C in Supporting Information S1).

Three additional discrete samples were collected on 7 June 2019 (1 week before the late freshet June campaign), two in the main branch of the Bolshoi Annui tributary, and one near station 11 (stations K01 to K03; Figure 1).

These samples were collected manually at the surface and only $c(O_2)$, pH, T were measured on site. These samples represent the nearest period to the peak of the freshet and thus are included for reference.

On 8 August 2019, we observed a phytoplankton bloom at station 5 at the confluence between Pantheleika and Kolyma Rivers (Figure 1). We collected water samples for all the parameters described above, as well as for the identification of phytoplankton communities.

Water discharge for the Kolyma was obtained from the Kolymsk-1 gauge station (Figure 1). For the Ambolikha, we used direct instantaneous discharge measurements measured between 28 June and 2 August 2019 using an acoustic doppler current meter (SonTek-SL 1500-3G, Xylem Inc., San Diego, CA, USA) that was mounted at the Ambolikha site at station 1 (Figure 1), see Castro-Morales, Canning, Körtzinger, et al. (2022) for details. We calculated integrated water residence times following Jones et al. (2017). The integrated water residence time (Supplement E in Supporting Information S1) is the average time that a water parcel takes to travel in the sampled channel segment. It is calculated from the cumulative sum of the discharge that passes through the upstream and downstream limits of the channel of interest. The water isotope signatures $\delta(^2H, H_2O)$ and $\delta(^{18}O, H_2O)$ were used to identify predominant water sources. Following Welp et al. (2005), we constructed the local meteoric water line based on endmember values for snow ($\delta(^{18}O, H_2O) = -26.2 \pm 5.0‰$) and rain ($\delta(^{18}O, H_2O) = -16.3 \pm 3.8‰$) collected near Chersky.

2.3. O_2/Ar Ratio Measurements and Gas Flux Calculations

Our study is the first application of the O_2/Ar ratios and the triple O_2 isotopologues in Arctic rivers. Because O_2 and Ar have similar solubility properties in water, and Ar has no biological sources or sinks, deviations of the O_2/Ar ratio from saturation (as a function of water temperature T and salinity S) reflect biological activity and are expressed as biological oxygen supersaturation $\Delta(O_2/Ar)$, that is, $\Delta(O_2/Ar) = c_{meas}(O_2/Ar)/c_{sat}(O_2/Ar) - 1$ (Craig & Hayward, 1987; Emerson et al., 1995; Kaiser et al., 2005). $\Delta(O_2/Ar)$ provides a measure of net community productivity that is gross productivity minus respiration. O_2 isotopologues further distinguish photosynthetic from atmospheric O_2: the latter has a relative ^{17}O-deficit from stratospheric isotope exchange reactions (Luz & Barkan, 2000; Luz et al., 1999), while photosynthetic O_2 reflects the isotopic composition of water, adjusted for photosynthetic isotopic fractionation, and shows a ^{17}O-excess relative to atmospheric O_2 (Eisenstadt et al., 2010; Kaiser & Abe, 2012). O_2 triple isotopologues have been widely used in marine productivity studies (e.g., Castro-Morales et al., 2013; Hendricks et al., 2005; Juranek & Quay, 2013; Luz & Barkan, 2000; Quay et al., 2010; Stanley et al., 2010), including the central Arctic Ocean (Eveleth et al., 2014; Ulfsbo et al., 2014), and the Beaufort Gyre (Stanley et al., 2015).

The first aliquot drawn from the Niskin bottle was dedicated for the O_2/Ar and oxygen isotopic analysis. A volume of 300 mL was transferred into pre-evacuated clear glass flasks fitted with high-vacuum valves (Glass Expansion) and previously spiked with 7 mg $HgCl_2$ to prevent biological activity after filling. The flasks were filled to 50 ± 25% of their volume and stored at room temperature in the dark until analysis at the University of East Anglia, UK. To avoid any air contamination of the sample or gas leak from the sample, the glass flasks were fitted with an extended neck that was filled with water to serve as additional seal during storage. Following Seguro et al. (2017), the water phase was removed from each flask under vacuum and the remaining gas phase sealed into glass tubes containing molecular sieve pellets. The gas phase was cryogenically and gas chromatographically purified to remove water vapor, N_2 and CO_2. A correction for headspace-water partitioning to derive the original dissolved gas concentration following Luz et al. (2002) was subsequently done. The remaining O_2/Ar mixture was transferred into a dual inlet mass spectrometer (Thermo Finnigan MAT 253) for quantification of O_2/Ar ratios (ion beam intensities at m/z 32 and m/z 40; by peak jumping) and O_2 isotopologue ratios $^{16}O^{17}O/^{16}O_2$ and $^{16}O^{18}O/^{16}O_2$ (Section 2.4). The relative standard deviation (1σ) of dry air aliquots measured between samples was 0.7‰ for O_2/Ar. The air-saturation concentrations $c_{sat}(O_2)$ and $c_{sat}(Ar)$ as a function of T and S were calculated following García and Gordon (1992) and Hamme and Emerson (2004). We derived the Ar supersaturation $\Delta(Ar)$ from $\Delta(O_2/Ar)$ and $\Delta(O_2)$ as:

$$\Delta(Ar) = \frac{\Delta(O_2) - \Delta(O_2/Ar)}{1 + \Delta(O_2/Ar)} \quad (1)$$

and the Ar concentration as:

$$c(\mathrm{Ar}) = c_{\mathrm{sat}}(\mathrm{Ar})[1 + \Delta(\mathrm{Ar})] \quad (2)$$

2.3.1. Gas Exchange Coefficients

The gas exchange coefficient k was calculated using three methods for comparison purposes (Section 3.4):

1. Empirical hydraulic model (Equation 7 in Table 2 of Raymond et al. (2012), short: R12; Supplement D1 in Supporting Information S1):

$$k_{\mathrm{R12}}/(\mathrm{m\ d^{-1}}) = \left(\frac{Sc}{600}\right)^{-0.5}\left[4725(V/\mathrm{m\ s^{-1}})\,s^{0.86} \times (Q/\mathrm{m^3 s^{-1}})^{-0.14} \times (D/\mathrm{m})^{0.66}\right] \quad (3)$$

   k_{R12} was adjusted to the Schmidt number (Sc) of O_2 as a function of temperature following Wanninkhof (1992, 2014). 600 is the Schmidt number of CO_2 and O_2 in freshwater at a temperature of 20 and 17.5°C, respectively, and it is commonly used for normalization of k values (Raymond et al., 2012). The river slope ($s = \Delta h/L$) and the flow velocity ($V = Q/DW$) are calculated from discharge Q, depth $D = 10$ m and channel width $W = 2$ km. For the Kolyma, $s = 0.003\%$, based on channel length $L = 120$ km and mean elevation change $\Delta h = 4$ m (Arctic DEM Explorer slope map; 2 m horizontal resolution; Environmental Systems Research Institute, Polar Geospatial Center; https://livingatlas2.arcgis.com/arcticdemexplorer/, last access: 7 October 2021). For the Ambolikha ($W = 0.05$ km), $s = 0.009\%$, based on channel length $L = 1.6$ km and $\Delta h = 1.5$ m between stations 1 and 4 (Figure 1).
2. Wind speed-based parameterization (Wanninkhof, 2014, short: W14; Supplement D2 in Supporting Information S1):

$$k_{\mathrm{W14}}/(\mathrm{m\ d^{-1}}) = \left(\frac{Sc}{660}\right)^{-0.5} \times 0.24 \times 0.251 \times (u_{10}/\mathrm{m\ s^{-1}})^2 \quad (4)$$

   In this formulation, the Schmidt number of O_2 or CO_2 is normalized to 660, which is the Sc for CO_2 in seawater at 20°C (Wanninkhof, 2014). Wind speed u was measured every 30 min at an eddy covariance tower located 8 m above the water surface near station 1 (Kittler et al., 2017). To obtain u_{10}, u was adjusted to 10 m above the water surface (Amorocho & Devries, 1980). We also calculated a weighted k value (k_w) to account for the variability of O_2 (and CO_2) in the top water column as a response to varying wind speeds over a certain period of time. k_w is the corrected k_{W14} using the method of Teeter et al. (2018) (Supplement D2 in Supporting Information S1).
3. Since argon is an inert gas, it can be used to calculate the gas exchange coefficient k_{Ar} in a quasi-Lagrangian fashion using its concentration gradient along the river channel, the distance of the transect and flow velocity. We derived k_{Ar} using the change in Ar concentration c(Ar) along the June transect in Kolyma from stations 6 to 24 (excluding stations 5, 10, 11, 18, 19 and 25, which were affected by tributaries), following Equations 5a–5d:

$$z_{\mathrm{mix}}\frac{\mathrm{d}c}{\mathrm{d}t} = -k(c - c_{\mathrm{sat}}) \quad (5a)$$

$$c - c_{\mathrm{sat}} = (c_0 - c_{\mathrm{sat},0})\,\mathrm{e}^{-\frac{kt}{z_{\mathrm{mix}}}} \quad (5b)$$

$$\ln\frac{c - c_{\mathrm{sat}}}{c_0 - c_{\mathrm{sat},0}} = -\frac{kt}{z_{\mathrm{mix}}} \quad (5c)$$

$$\ln\frac{\Delta}{\Delta_0} + \ln\frac{c_{\mathrm{sat}}}{c_{\mathrm{sat},0}} = -\frac{kt}{z_{\mathrm{mix}}} \quad (5d)$$

For clarity, the label "Ar" has been omitted from c, k and Δ. z_{mix} is the mixed layer depth of 10 m (corresponding to the mean full river depth D), c_0 is the Ar concentration at the upstream end of the June transect, c_{sat} is the Ar concentration at air saturation. We replace time t with the distance along the transect (Δd), since $\Delta d = Vt$, with the water flow velocity, $V = Q/DW = 0.67$ m s^{-2}. Thus, we have:

$$\ln\frac{\Delta}{\Delta_0}+\ln\frac{c_{sat}}{c_{sat,0}}=-\frac{kW\Delta d}{Q} \tag{5e}$$

The slope of a linear regression of the left side of Equation 5e against Δd, divided by Q/W, gives k_{Ar} for the entire transect.

2.3.2. Air-Water Gas Exchange Flux Densities

We calculated air water gas exchange flux densities F_a of CO_2, O_2 and so-called biological O_2 in units of mmol m^{-2} d^{-1} from the gas exchange coefficient and the concentration gradient c-c_{sat}, where c is the measured concentration and c_{sat} is the air-saturation concentration in equilibrium with the atmosphere:

$$F_a(O_2)=k(O_2)\,[c(O_2)-c_{sat}(O_2)] \tag{6a}$$

$$F_a(CO_2)=k(CO_2)\,[c(CO_2)-c_{sat}(CO_2)] \tag{6b}$$

Positive values correspond to emissions from the river to the atmosphere.

The biological O_2 flux density, $F_{bio}(O_2)$ is defined as:

$$F_{bio}(O_2)=F_a(O_2/Ar)=k(O_2)\,c_{sat}(O_2)\Delta(O_2/Ar) \tag{6c}$$

The symbol $F_{bio}(O_2)$ has often been used in the past (Castro-Morales et al., 2013; Kaiser et al., 2005), but for consistency with the advective flux symbol $F_{adv}(O_2/Ar$; see below), we prefer $F_a(O_2/Ar)$ here.

2.3.3. Advective Gas Flux Densities and Net Community Production

Diel changes in gas concentrations are expected to be small because of deep mixed layers and long gas residence times with respect to atmosphere-water exchange. We have therefore neglected them. However, we account for horizontal (along-river) gradients by adopting a similar quasi-Lagrangian approach to that used with the $c(Ar)$ gradient to derive k_{Ar}. Thus, we can estimate an advective flux F_{adv} (Seguro et al., 2023) from the gradients in the O_2, CO_2 and biological O_2 concentrations and the ratio of discharge Q to river width W:

$$F_{adv}=z_{mix}\frac{dc}{dt}=z_{mix}V\frac{dc}{dx}=\frac{Q}{W}\frac{dc}{dx} \tag{7}$$

The gradient dc/dx is derived by linear regression of concentrations against transect distance, excluding stations influenced by tributaries. Positive values correspond to a concentration increase from upstream to downstream.

Net community productivity is calculated as:

$$N(O_2/Ar)=F_a(O_2/Ar)+F_{adv}(O_2/Ar) \tag{8a}$$

$$N(O_2)=F_a(O_2)+F_{adv}(O_2) \tag{8b}$$

$$N(CO_2)=-F_a(CO_2)-F_{adv}(CO_2) \tag{8c}$$

2.4. Gross Oxygen Productivity ($G(^{17}O)$) From O_2 Triple Isotopologues

We estimated gross photosynthetic oxygen productivity ($G(^{17}O)$) from the stable isotope composition of dissolved O_2 (Luz & Barkan, 2000; Luz et al., 1999), the gas transfer velocity $k(O_2)$ and the downstream gradients in the isotope deltas. Just as net community productivity (Equation 8a), $G(^{17}O)$ is the sum of the gas-exchange flux density F_a (^{17}O) and the advective flux density $F_{adv}(^{17}O)$, as defined in Equations 10 and 11:

$$G(^{17}O)=F_a(^{17}O)+F_{adv}(^{17}O) \tag{9}$$

As explained in the introduction, the observed $^{17}O/^{16}O$ and $^{18}O/^{16}O$ variations in the dissolved O_2 pool can be used to determine the relative contributions of photosynthetic and atmospheric O_2. The isotope ratio variations are expressed as isotope deltas, $\delta(^{17}O, O_2$; short: $^{17}\delta$) and $\delta(^{18}O, O_2)$ (short: $^{18}\delta$), with $^{17}\delta$ and $^{18}\delta$ defined as $\delta = R_{sample}/R_{standard} - 1$, where R refers to the isotope number ratios $N(^{17}O)/N(^{16}O)$ or $N(^{18}O)/N(^{16}O)$ of sample (dissolved O_2) and standard (O_2 in tropospheric dry air).The relative standard deviation (1σ) of dry air aliquots measured between samples was 0.010‰ for $^{17}\delta$, 0.016‰ for $^{8}\delta$ and 0.005‰ for the ^{17}O excess, defined as $\Delta(^{17}O) = {}^{17}\delta - 0.5179\ {}^{18}\delta$ (Kaiser, 2011a).

To calculate $F_a(^{17}O)$, we followed the dual-delta method (Kaiser, 2011a):

$$F_a(^{17}O) = k(O_2)\, c_{sat}(O_2)\, \frac{\left(1 + {}^{17}\varepsilon_E\right)\frac{{}^{17}\delta - {}^{17}\delta_{sat}}{1 + {}^{17}\delta} - \gamma_R\left(1 + {}^{18}\varepsilon_E\right)\frac{{}^{18}\delta - {}^{18}\delta_{sat}}{1 + {}^{18}\delta} + \Delta(O_2)\left({}^{17}\varepsilon_E - \gamma_R\, {}^{18}\varepsilon_E\right)}{\frac{{}^{17}\delta_P - {}^{17}\delta}{1 + {}^{17}\delta} - \gamma_R \frac{{}^{18}\delta_P - {}^{18}\delta}{1 + {}^{18}\delta}} \quad (10)$$

The δ values of dissolved O_2 at air-saturation for ^{17}O and ^{18}O depend on water temperature: $^{18}\delta_{sat} = e^{-0.00072951 + 0.42696\ K/T} - 1$ (Benson et al., 1979); $^{17}\delta_{sat}$ is calculated from $^{18}\delta_{sat}$ as $^{17}\delta_{sat} = (1 + {}^{18}\delta_{sat})^{0.518}\ e^{(0.6\theta/°C + 1.8)/ppm} - 1$, with the water temperature θ in °C (Luz & Barkan, 2009). The kinetic isotope fractionation during O_2 invasion for ^{18}O ($^{18}\varepsilon_I$) is calculated as function of $^{18}\delta_{sat}$ and the kinetic isotope fractionation during O_2 evasion, $^{18}\varepsilon_E = -2.8‰$, (Knox et al., 1992) as $^{18}\varepsilon_I = (1 + {}^{18}\varepsilon_E)\ (1 + {}^{18}\delta_{sat}) - 1$ (Kaiser, 2011a, 2011b). The $^{17}O/^{16}O$ kinetic isotope fractionation during O_2 invasion ($^{17}\varepsilon_I$) is calculated as $^{17}\varepsilon_I = (1 + {}^{18}\varepsilon_I)^{0.516} - 1$ (Kaiser, 2011a). The ratio of the $^{17}O/^{16}O$ to $^{18}O/^{16}O$ respiratory fractionation is $\gamma_R = {}^{17}\varepsilon_R/{}^{18}\varepsilon_R = 0.5179$; obtained from experiments covering temperature range of 17–37°C and different organisms (Luz & Barkan, 2005). $^{17}\delta_p$ and $^{18}\delta_p$ are the photosynthetic end-members calculated as $\delta_p = [1 + \delta(H_2O)]\ (1 + \varepsilon_p) - 1$ (Kaiser & Abe, 2012). For $^{18}\delta_p$, we used river $\delta(^{18}O, H_2O)$ and the photosynthetic isotopic fractionation $^{18}\varepsilon_p = 4.426‰$ of the diatom *Phaeodactylum tricornutum* (Eisenstadt et al., 2010; Kaiser & Abe, 2012), which can live in both seawater and freshwater (Listwan et al., 2018). We assumed that $\delta(^{17}O, H_2O) = [1 + \delta(^{18}O, H_2O)]^{0.528} + 0.000033$ followed the global meteoric water line (Luz & Barkan, 2010). This assumption agrees with a recent review of this method in the hydrological cycle (Aron et al., 2021) and deviations to this relationship generally occur beyond the range $\delta(^{18}O, H_2O) > -15‰$.

Finally, $^{17}\delta_p$ was calculated from $\delta(^{17}O, H_2O)$ and $^{17}\varepsilon_p = 2.314‰$ (Eisenstadt et al., 2010; Kaiser & Abe, 2012). To calculate $F_{adv}(^{17}O)$ we use a slightly adapted version of Kaiser's Equation 42 (Kaiser, 2011a):

$$F_{adv}(^{17}O) = \frac{Q}{W} c(O_2)\, \frac{\frac{d\left[\ln\left(1 + {}^{17}\delta\right) - \gamma_R \ln\left(1 + {}^{18}\delta\right)\right]}{dx}}{\frac{{}^{17}\delta_P - {}^{17}\delta}{1 + {}^{17}\delta} - \gamma_R \frac{{}^{18}\delta_P - {}^{18}\delta}{1 + {}^{18}\delta}} \quad (11)$$

The isotope delta terms in the numerator have been combined to ensure that the uncertainty resulting from the linear regression against transect distance is not double-counted. The time–space transformation is done as in Equation 7 using the ratio of discharge Q and river width W.

2.5. Dissolved Organic Matter Characterization

For DOM characterization, 500 mL of water was filtered through a pre-combusted GF/F filter mounted in a filtration unit with a hand pump. The filtrate was collected in acid-washed HDPE brown bottles and stored at 4°C. For solid-phase extraction (SPE), the filtrate was passed through an Oasis HLB cartridge at pH 7.0 to avoid hydrolysis (Waters, Germany). The organic matter was eluted with 4 mL of methanol (Koch & Dittmar, 2006).

An electrospray ionization (ESI) high-resolution Orbitrap mass spectrometer (HR-ESI-MS, QExactive, Thermo Scientific, USA) was used to gather high-resolution spectra ($m/\Delta m = 280{,}000$ at m/z 200) for Ambolikha DOM samples ($n = 40$; analyzed in triplicate) in the range m/z 150–700. The device was externally calibrated using a calibration solution (Proteomass ESI, Sigma-Aldrich, USA). Methanol extracts were randomized, and equivalent DOC concentrations (9 mg L^{-1}) were infused directly into the ESI source (injection volume: 20 µL) and evaluated in negative ionization mode (Kügler et al., 2019). The average mass spectrum was made up of 100 successive

images. Using OpenMS v.2.6.0, the spectra were internally calibrated by DOM ions found in all samples (Röst et al., 2016) to keep the analytical mass error <2 ppm. When a signal appeared in all sample triplicates, it was considered present. The average signal intensity was used for subsequent statistical analysis (Supplement B and Appendix files A1–A3 in Supporting Information S1).

2.6. Composition of Microbial Communities

The collection, processing, extraction, and analysis of the samples collected for microbial community composition have been described by Castro-Morales, Canning, Körtzinger, et al. (2022). The only difference was the use of the µgreen-db database to classify phototrophs. Supplement C in Supporting Information S1 contains further details on the methodology for gene amplification and sequencing.

2.7. Statistical Analysis

We performed a principal component analysis (PCA) with the water parameters at the station level to identify the most dominant parameters in terms of their contribution to the variance in the data set and to reveal correlations between the parameters. This was followed by linear correlation analysis with a p-value <0.05 among selected main parameters. A Wilcoxon rank sum test with a significance level of 5% was done to identify statistically significant relations among the seasons and transects.

For DOM signature analysis, a principal coordinate analysis (PCoA) was performed to explore the overall structure of the data, supported by a canonical analysis and hierarchical cluster analysis (HCA), to define and label distinct sample groups of stations based on molecular formulas identified in DOM (for details see Supplement B in Supporting Information S1). These groupings support and complement the quantitative correlations observed in the water's biochemical parameters across stations. These groups confirm quantitative correlations in the water biochemical parameters for the different stations. Results of each analysis are shown in the corresponding results section below. We calculated the average ±1 standard deviation of the CO_2 and O_2 flux densities during the late freshet, the base flow period and bloom event per river and group of corresponding stations (Table 3).

3. Results

3.1. Continuous Gas Measurements Along River Transects in June (Late Freshet)

Continuous measurements were only performed during the river transects in June. Therefore, a comparison of results between different seasons is restricted to the discrete sampling (see below). Large differences in the water properties, confirmed by statistically significant differences (Wilcoxon rank-sum test, $p < 0.05$) were observed between the Kolyma upstream and downstream transects, and the Kolyma and Ambolikha upstream transects (Figure 2). Table 1 shows the average ±1 standard deviation of the continuously measured parameters along these transects. The Kolyma was on average 5°C colder than the Ambolikha, had nearly double its conductivity (κ), and a much higher average O_2 supersaturation of $\Delta(O_2) = 11.3\%$ than the Ambolikha $\Delta(O_2)$ of −30.5% (Table 1).

The $p(CO_2)$ in both rivers was always above atmospheric $p(CO_2)$ (global average for June 2019: 409.4 µatm; Dlugokencky (2019)), but the average Ambolikha $p(CO_2)$ of 5162 ± 530 µatm was three times higher than the Kolyma average of 1,632 ± 274 µatm (Table 1).

The spatial distribution of the Kolyma $p(CO_2)$ shows hot spots at the confluence with tributaries (Figures 2a and 2b). These hotspots represent small regions but have $p(CO_2)$ values 1.5 and 2 times higher (between 2,200 and 3,200 µatm) than elsewhere (average: 1,500 µatm). The Ambolikha $p(CO_2)$ maximum of 5,800 µatm was found in the headwaters (Figure 2e).

To investigate the spatial distribution of $p(CO_2)$ and $c(O_2)$ along the transects, we determined the linear correlations between pairs of parameters. Table 2 shows linear coefficients of determination R^2 ($p < 0.05$) of $p(CO_2)$ and $c(O_2)$ to other water parameters in June 2019.

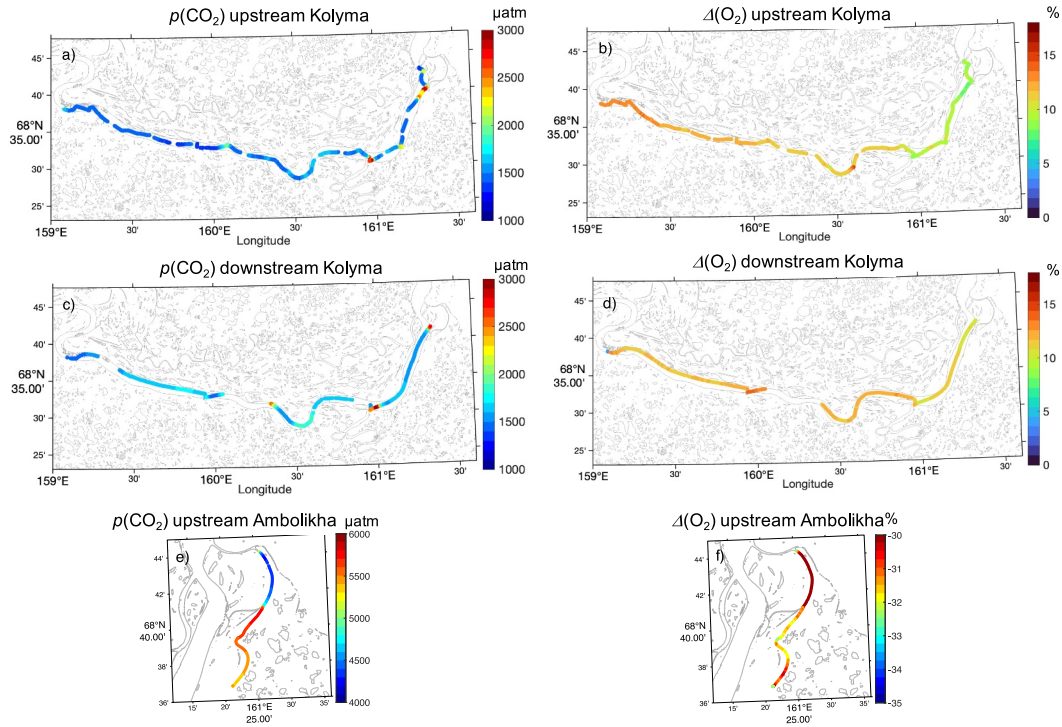

Figure 2. Continuous measurements in June of $p(CO_2)$ (panels a, c, and e) and oxygen supersaturation $\Delta(O_2)$ (panels b, d, and f) along the Kolyma upstream (a, b) and downstream (c, d) transects, and Ambolikha (e, f) upstream transect. Panels (a, c) for $p(CO_2)$, as well as (b, d) for $\Delta(O_2)$ share the same color scale. Each data point represents an average of 1 min of continuous measurements.

3.2. Temporal Comparison of Water Properties at Station Level

We compared water properties between the late freshet (June) and the low-flow period (August) across all stations (Figure 1). Strong seasonal contrasts were observed in T, fDOM concentration, nutrients, oxygen and CO_2 (Figure 3). In both rivers, T dropped by 3–6°C between June and August, though the Ambolikha remained 3–5°C warmer than the Kolyma (Figure 3a). Residence time doubled from 1 to 2 days (Supplement E in Supporting Information S1). DOC and fDOM concentrations were roughly twice as high in June, reflecting higher inputs during freshet, while pCO2 was nearly four times higher in Kolyma (2,293 ± 1,450 μatm vs. 615 ± 307 μatm), and decreased nearly 10 times in Ambolikha (5,800 μatm vs. 626 μatm; Figure 3k). By August, $c(O_2)$ rose substantially, particularly in the Ambolikha (196 μmol L^{-1} in June to 331 μmol L^{-1} in August; Figure 3j), and pH increased by 0.7 in parallel with declining $p(CO_2)$ (Figures 3f and 3k).

Table 2
Linear Coefficient of Determination R^2 (Statistically Significant at $p < 0.05$) From the Most Representative Relationships in Continuously Measured Water Parameters in the Kolyma and Ambolikha Rivers During June 2019

	Kolyma upstream (n = 1116)	Kolyma downstream (n = 450)	Ambolikha (n = 113)
$p(CO_2)$ versus $c(O_2)$	(−) 0.61	(−) 0.44	(−) 0.89
$p(CO_2)$ versus κ	(−) 0.41	(−) 0.28	(−) 0.88
$p(CO_2)$ versus T	(+) 0.22	(+) 0.47	(+) 0.71
$p(CO_2)$ versus fDOM concentration	(+) 0.37	(+) 0.47	(+) 0.93
$c(O_2)$ versus T	(−) 0.29	(−) 0.65	(−) 0.84
$c(O_2)$ versus fDOM concentration	(−) 0.24	(−) 0.13	(−) 0.93

Note. n: number of 1-min average data points.

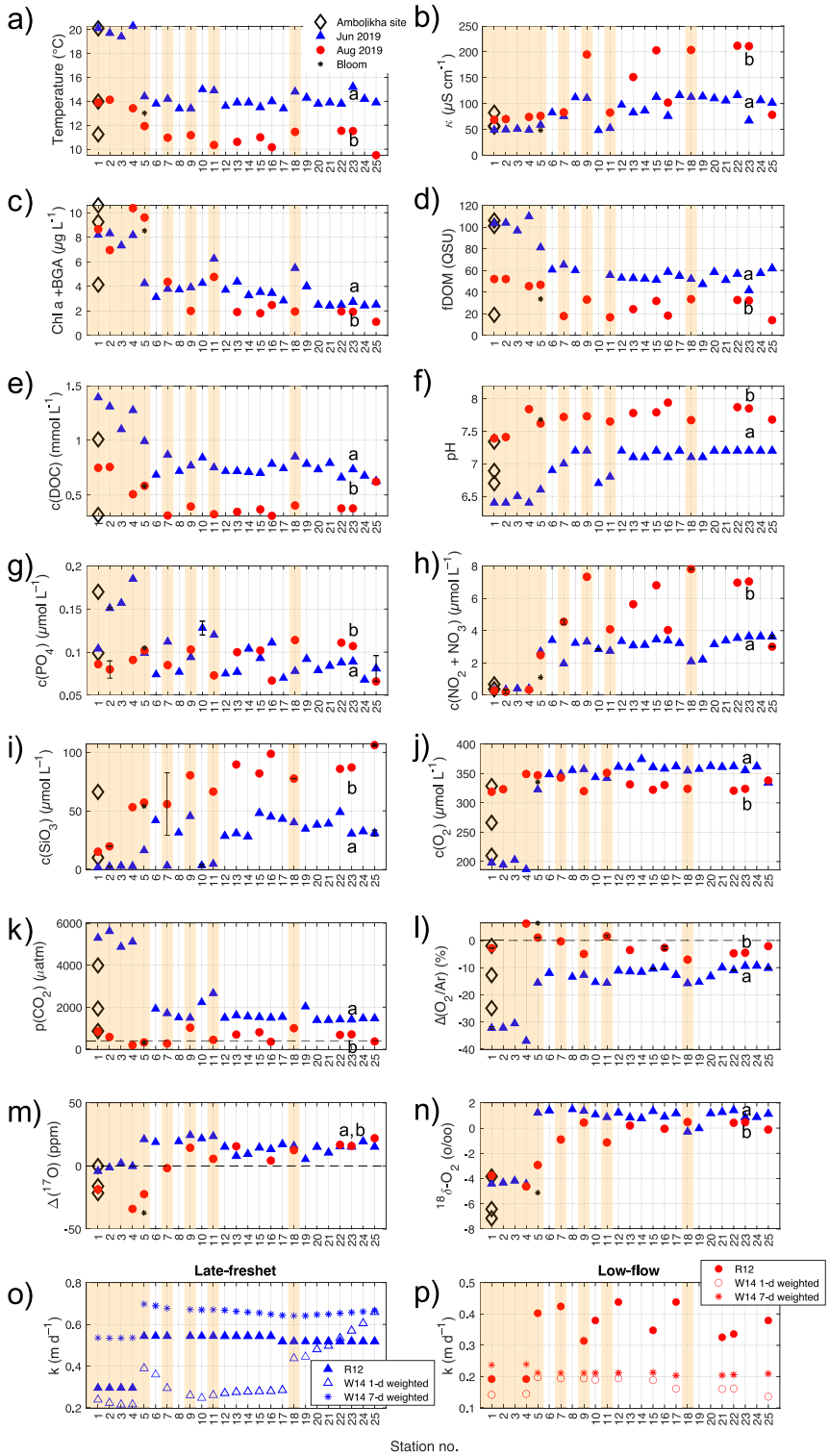

Figure 3. Water properties in Ambolikha (stations 1–4) and Kolyma (stations 5–25) during June (blue triangles) and August (red circles) 2019. The orange shade highlights the stations at or near tributaries (1–4 in Ambolikha, and 5, 7, 9 and 11 in Kolyma, and 18 inside Leonid's channel). Diamonds at station 1 (Ambolikha site, Figure 1) were sampled between June and August to monitor the seasonal transition. The black star at station 5 are measurements from the bloom on 8 August 2019. Error bars for the nutrients concentrations results (g to i) represent 1σ of sample replicates. Because the location of station 23 differed slightly between June and August, letters (a and b) are assigned, respectively (Figure 1).

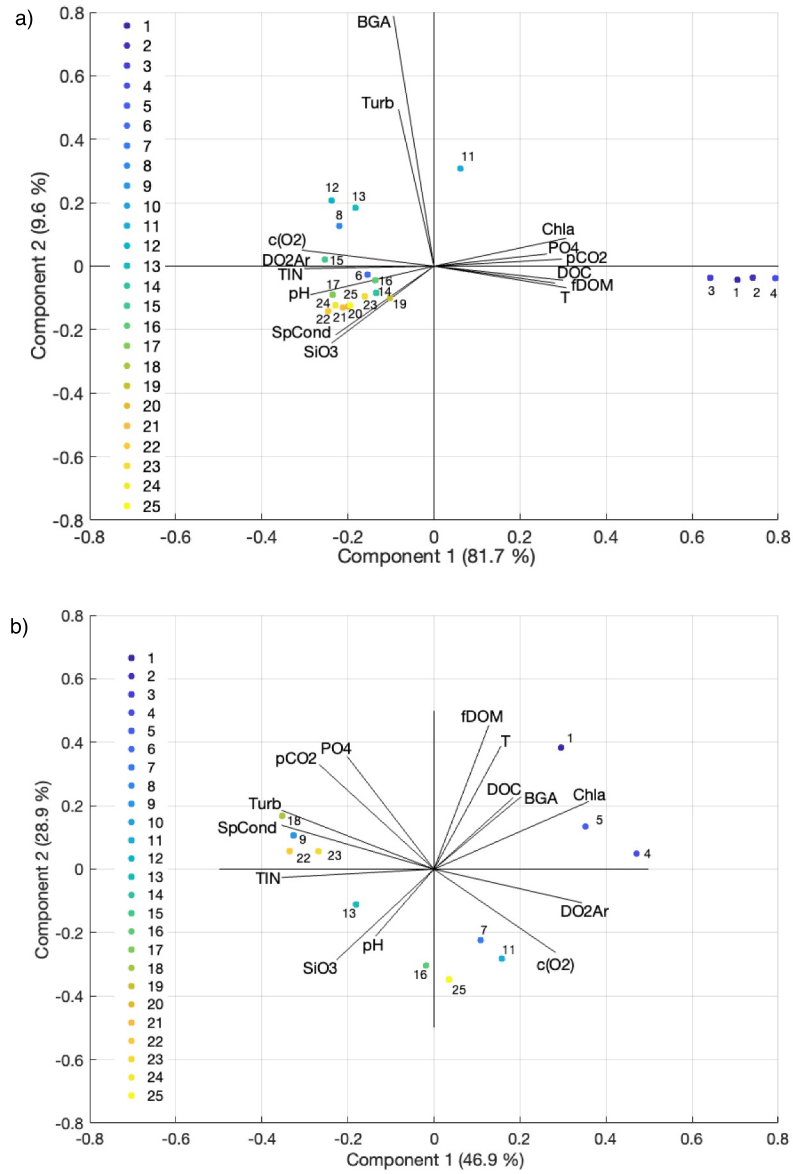

Figure 4. Principal component analysis of scaled chemical and physical water properties at stations 1–25 in Kolyma and Ambolikha Rivers in 2019 during (a) June late-freshet and (b) August low-flow period. Stations are identified by color and number next to the symbols. The first two components explained 91% and 76% of the variability in June and August, respectively.

Nutrient dynamics differed between rivers. In the Kolyma, $c(NO_x^-)$ and $c(SiO_3^{2-})$ increased from June to August (Figures 3h and 3i), while $c(PO_4^{3-})$ decreased at stations 7, 11 and 16 (Figure 3g). In contrast, the Ambolikha showed little change in $c(NO_x^-)$ (Figure 3h), but $c(PO_4^{3-})$ decreased half from June to August (Figure 3g). Average fDOM concentration and c(DOC) were twice as high in June as in August (Figures 3d and 3e).

The principal component analysis (PCA) supported these patterns, with conditions in June characterized by a positive correlation between c(DOC), fDOM concentration, T, $p(CO_2)$, $c(PO_4^{3-})$ and c(Chl a). These parameters correlated negatively with $c(O_2)$, pH, κ, $c(NO_x^-)$, $c(SiO_3^{2-})$ and $\Delta(O_2/Ar)$ (Figure 4a). Negative correlations were found for $p(CO_2)$ versus pH, $c(O_2)$ and $\Delta(O_2/Ar)$ ($R^2 > 0.90$). $c(O_2)$ and $\Delta(O_2/Ar)$ also correlated negatively with c(Chl a) ($R^2 = 0.87$ and 0.93). This decoupling of $c(O_2)$ variations from c(Chl a) could be due to dominant

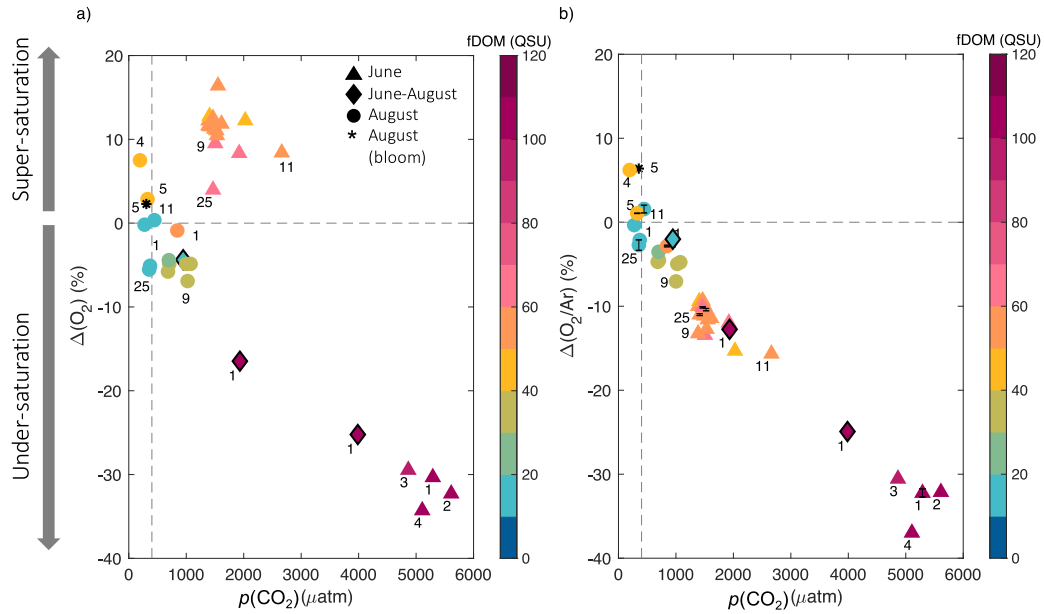

Figure 5. Plot of (a) O_2 supersaturation $\Delta(O_2)$ and (b) biological O_2 supersaturation $\Delta(O_2/Ar)$ versus $p(CO_2)$ in June (triangles) and August (circles). Vertical dashed line: atmospheric $p(CO_2)$ in June (409.4 μatm). Black-edged diamonds: seasonal transition at station 1 (Ambolikha Site). Black star: station 5 during August bloom. Color bar: fDOM concentration. Station numbers are added next to the symbols.

respiration processes compared to production. Ambolikha stations 1–4 form a cluster in June, while stations 15–25 in the upper Kolyma grouped closely. Stations 8, 11, 12, and 13 are isolated, highlighting distinct characteristics of stations near the outlet of tributaries (Figure 4a). The August biplot (Figure 4b) showed weaker but shifted correlations, for example, c(Chl a) versus $\Delta(O_2/Ar)$ and $c(O_2)$ (R^2 = 0.57 and 0.19) now positively correlated, indicating greater biological influence on $c(O_2)$ and biomass.

During August in the low-flow period, a pronounced phytoplankton bloom was detected (Figure S2 in Supporting Information S1). Vertical profiles measured with the EXO2 sonde pre-bloom (5 August) and during the bloom (8 August) revealed that during the bloom, c(Chl a) formed distinct subsurface maxima reaching values five times higher (28 μg L^{-1}) than surrounding waters (6 μg L^{-1}). This bloom coincided with a decrease in turbidity, fDOM concentrations, and $c(O_2)$ (Figure S2b in Supporting Information S1). Elevated $\Delta(O_2/Ar)$ values (discrete sample from 1 m depth), missed the c(Chl a) maximum (located at 0.25 and 0.48 m depth), but were 5.3% higher than pre-bloom conditions and may represent a lower bound to the biologically produced oxygen during the bloom (Figures 3 and 6). During the bloom, c(Chl a) and c(BGA) reached nearly double their June values (Figure 3c). $p(CO_2)$ decreased by 21 μatm between 5 and 8 August, and in the same period conductivity and turbidity decreased from 76 to 48 μS cm^{-1} and from 11 to 5.5 FNU, respectively. The hydrograph at station Kolymsk-1 showed that during these 3 days the river discharge decreased from 6.4×10^3 to 4.8×10^3 m^3 s^{-1} (Figure S1 in Supporting Information S1). During the bloom event, $c(SiO_3^{2-})$ declined by 3 μmol L^{-1}, and $c(NO_x^-)$ decreased by 1.4 μmol L^{-1} compared to pre-bloom conditions (Figures 3i and 3h), indicating uptake of these nutrients during the bloom. The stoichiometric ratio of the increase in biological O_2 concentration (by 12.4 μmol L^{-1}) to the $c(NO_x^-)$ drawdown (ratio of 8.9) from pre-bloom to bloom conditions, was consistent with phytoplankton uptake near the canonical Redfield ratio for O_2:N being 8.6 ± 1.0 (Li & Peng, 2002).

3.3. Biological O_2 Saturation as an Indicator of Biological Oxygen Productivity

To identify biologically produced O_2, we compared $\Delta(O_2)$ and $\Delta(O_2/Ar)$ versus $p(CO_2$; Figure 5). In June, both rivers were biologically oxygen-depleted, with strongly negative $\Delta(O_2/Ar)$ (−32.9%) in the Ambolikha (mostly from biological O_2 removal as average $\Delta(O_2)$ = −31.7%), and moderately negative values in the Kolyma

Table 3
Summary of Average ±1 Standard Deviation of CO_2 and O_2 Flux Densities

	Period	Late freshet (June)		Low flow (August)		Bloom (August)
	River (stations)	Ambolikha (1–4)	Kolyma (5–25)	Ambolikha (1–4)	Kolyma (5–25)	Kolyma (5)
Row	Flux densities in mmol m^{-2} d^{-1} (negative: loss or uptake from atmosphere, positive: production or emission)					
1	$F_a(CO_2)$	57 ± 4	27 ± 8	1 ± 4	3 ± 5	−1 ± 1
2	$F_a(O_2)$	−28 ± 2	17 ± 5	2 ± 3	−3 ± 3	2 ± 1
3	$F_a(O_2/Ar)$	−30 ± 3	−20 ± 4	1 ± 4	−3 ± 3	6 ± 3
4	$F_a(^{17}O)$	6 ± 2	−5 ± 4	43 ± 27	4 ± 18	141 ± 70
5	$F_{adv}(CO_2)$	−24 ± 28	86 ± 22	−25 ± 13	−38 ± 41	−1 ± 1
6	$F_{adv}(O_2)$	−14 ± 15	−34 ± 26	25 ± 13	29 ± 19	−11 ± 6
7	$F_{adv}(O_2/Ar)$	−20 ± 20	−17 ± 16	27 ± 14	34 ± 19	11 ± 6
8	$F_{adv}(^{17}O)$	−10 ± 7	−34 ± 37	46 ± 30	46 ± 35	40 ± 37
9	$N(CO_2$; Equation 8c)	−33 ± 28	−112 ± 23	24 ± 13	34 ± 41	3 ± 1
10	$N(O_2$; Equation 8b)	−42 ± 15	−18 ± 27	27 ± 13	26 ± 20	−9 ± 6
11	$N(O_2/Ar$; Equation 8a)	−50 ± 20	−37 ± 16	28 ± 14	31 ± 19	17 ± 7
12	$G(^{17}O$; Equation 9)	−4 ± 7	−39 ± 37	88 ± 41	49 ± 39	181 ± 79
13	R	46 ± 22	−3 ± 41	60 ± 43	18 ± 43	163 ± 79

Note. F_a values were calculated using k_{R12}. Respiration (Row 13) is calculated as $R = G(^{17}O) - N(O_2/Ar)$.

(−12.3%). The dominating melt and upstream water in this river during the high discharge period was oxygen-depleted. The Kolyma $\Delta(O_2)$ was however positive (average: 10.3%; Figure 5a).

By August, $p(CO_2)$ and $\Delta(O_2)$ decreased in both rivers (to 615 µatm and −7.7%, respectively), shifting toward saturation as water temperature dropped by 3.5°C on average (Figure 5a). $\Delta(O_2/Ar)$ increased on average by 10% in both rivers, shifting conditions toward saturation. The Ambolikha showed a transition to positive $\Delta(O_2)$ and $\Delta(O_2/Ar)$, mostly in station 4 near the confluence with the Pantheleika River (Figures 3l and 5b). The Kolyma remained undersaturated ($\Delta(O_2/Ar) = -2.9\%$), except at tributary confluences, that is, at station 5 (confluence with the Pantheleika) with 1.5%, and 1.6% at station 11 (confluence with the Bolshoi Anui and Malyi Anui).

Microbial community data supported these patterns (Figures S4b and S4c in Supporting Information S1). Photosynthetic bacteria in June were 0.1%–0.5% of the total community in the Ambolikha, and five times more abundant than in the Kolyma (0.03%–0.09%). These proportions increased fifty-fold by August, reaching 14% of the community in the Ambolikha, while remaining <1% in the Kolyma.

3.4. Net Community Productivity Derived From $\Delta(O_2/Ar)$

The calculated k_{R12} values for oxygen during the late-freshet (0.46 ± 0.07 m d^{-1}) were similar to k_{W14} (0.50 ± 0.33 m d^{-1}), while wind-weighted estimates $k_{weighted}$ ranged from 0.34 ± 0.12 m d^{-1} to 0.61 ± 0.02 m d^{-1}. For the low-flow period, k_{R12} decreased (0.30 ± 0.06 m d^{-1}), but were about twice the k values derived from wind speed: 0.14–0.18 m d^{-1} (Figures 3o and 3p). Estimates from Ar concentrations (k_{Ar} = 0.63 ± 0.44 m d^{-1}, at the average in situ temperature of 13.8°C, corresponding to $Sc(Ar) = 766$) were comparable. For flux density calculations, we used k_{R12}. The average air-sea (F_a) and advective fluxes (F_{adv}) for the different gases (CO_2, O_2, O_2/Ar and ^{17}O) in Kolyma and Ambolikha during the late freshet and low flow, including the bloom, are shown in Table 3 in rows 1 to 8. The average net ecosystem production ($N(O_2/Ar)$), gross oxygen productivity ($G(^{17}O)$) and respiration (R) are shown in Table 3 in rows 9 to 13.

In June, both rivers were net heterotrophic. Negative $\Delta(O_2/Ar)$, with Kolyma fluxes of $F_a(O_2/Ar) = -20 \pm 4$ mmol m^{-2} d^{-1} and $F_{adv}(O_2/Ar) = -17 \pm 16$ mmol m^{-2} d^{-1} (Figure 5, Table 3, row 3), yielding $N(O_2/Ar) = -37 \pm 16$ mmol m^{-2} d^{-1} (Table 3, rows 3, 7 and 11). Ambolikha, was even more undersaturated with $F_a(O_2) = -28 \pm 2$ mmol m^{-2} d^{-1} and $F_a(O_2/Ar) = -30 \pm 3$ mmol m^{-2} d^{-1}.

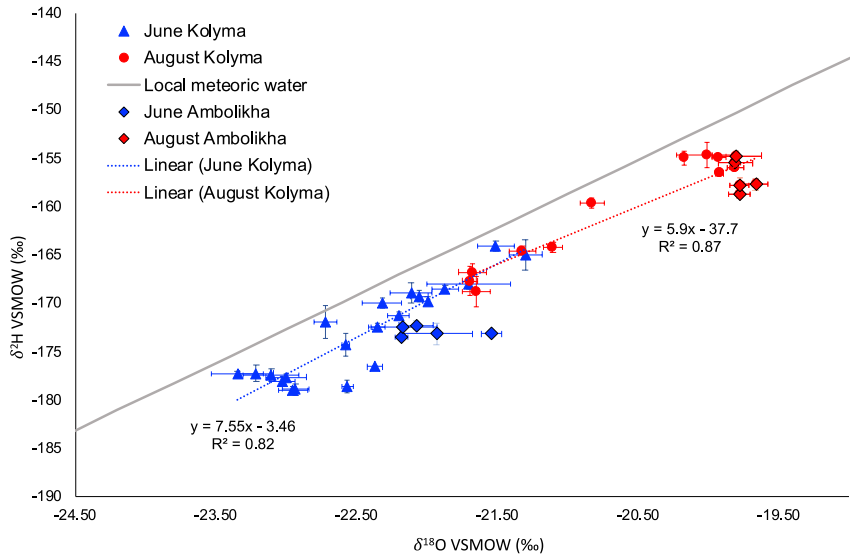

Figure 6. Isotopic composition of water $\delta(^{18}O, H_2O)$ against $\delta(^{2}H, H_2O)$. Blue symbols: late freshet (June) in Kolyma (filled triangles) and in Ambolikha (filled diamonds). Red symbols: low flow (August) in Kolyma (filled circles) and in Ambolikha (filled diamonds). The meteoric water line is shown with end members from Welp et al. (2005) measured in Kolyma samples. Error bars: standard deviation of three replicates.

By August, both rivers shifted toward net autotrophy (Table 3, rows 2 and 3, Figure 5). Ambolikha $F_a(O_2/Ar)$ rose to 1 ± 4 mmol m^{-2} d^{-1}, while Kolyma also moved toward saturation with average $F_a(O_2/Ar)$ = −3 ± 3 mmol m^{-2} d^{-1}. However, positive values were found at tributary confluences in stations 4, 5 and 11 (Figure 1) with $F_a(O_2/Ar)$ of 4, 1 and 2 mmol m^{-2} d^{-1}, respectively, and six times higher during the bloom at station 5 (6 mmol m^{-2} d^{-1}; Table 3, row 3). Advective fluxes $F_{adv}(O_2/Ar)$ also shifted from negative in June to positive in August (Ambolikha: −20 ± 20 mmol m^{-2} d^{-1} to 27 ± 14 mmol m^{-2} d^{-1}; Kolyma: −17 ± 16 mmol m^{-2} d^{-1} to 34 ± 19 mmol m^{-2} d^{-1} (Table 3, row 7). This resulted in positive net biological production $N(O_2/Ar)$ in August (Ambolikha: 28 ± 14 mmol m^{-2} d^{-1}; Kolyma: 31 ± 19 mmol m^{-2} d^{-1}). At the bloom site, $N(O_2/Ar)$ = 17 ± 7 mmol m^{-2} d^{-1} (Table 3, row 11), being half the river average.

Ar supersaturation Δ(Ar) was pronounced in June, averaging 26 ± 4% in Kolyma, but much lower in Ambolikha (2.7 ± 1.9%). Increases in Δ(Ar) tracked water warming, for example, at station 11, T = 7.7°C and Δ(Ar) = 0.8% (station K-03) 9 days prior to the upstream transect, and rose to 14.9°C with Δ(Ar) to 25.4% during the transect measurements in warmer conditions. Air temperatures increased over the same period of 9 days from 8.9 to 28.2°C. The warming of the water alone explains a 17.8% increase in Δ(Ar). Warming and gas fluxes are likely decoupled in this system because of the low gas exchange coefficients of 0.5 m d^{-1} resulting in exchange time scales of the order of 20 days (given a 10 m deep water column) and with most of the warming in Arctic rivers being due to shortwave radiative heating rather than sensible heat fluxes (King et al., 2016; Schmid & Read, 2022). The remainder of the Ar concentration increase of 7.7% may reflect injection of air from melting ice.

Lower Ambolikha Δ(Ar) values in June reflected slower flow (6 times lower) and longer equilibration times with respect to gas exchange. By August, Δ(Ar) approached saturation (0.0 ± 1.8%; Figure S4 in Supporting Information S1).

3.5. Isotopic Signals in Water and Dissolved Oxygen as Indicators of Water Sources and Gross Productivity

Our results showed a shift from more depleted values of $\delta(^{18}O, H_2O)$ = −22.4 ± 0.5‰ and $\delta(^{2}H, H_2O)$ = −173.0 ± 4.4‰ in June to −20.6 ± 0.8‰ and −161.1 ± 5.4‰ in August. This pattern and seasonal shift followed a line parallel to the meteoric water line (Figure 6). This confirms the snowmelt signal during the late freshet in June. In August, conductivity increased at most Kolyma stations (Figure 3b). Water isotope deltas also increased and got closer to the rainwater end member (Figure S3 in Supporting Information S1). These results

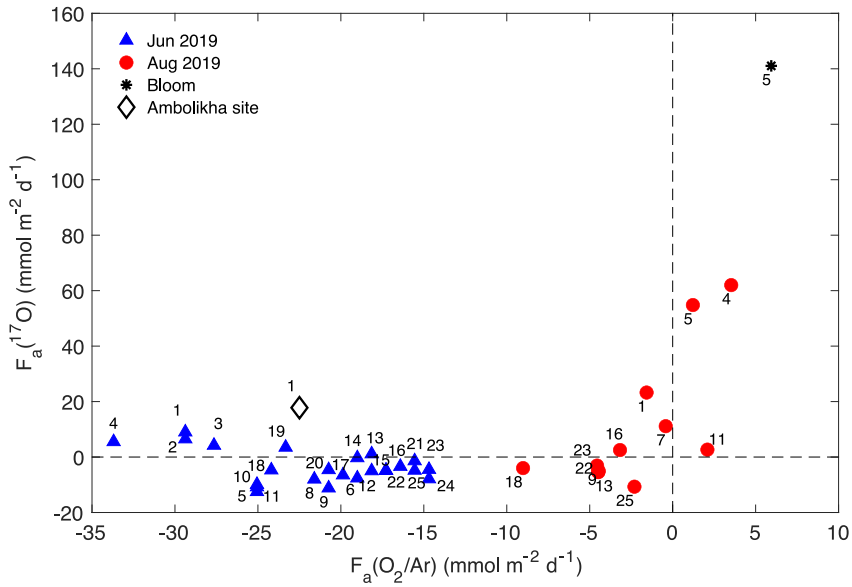

Figure 7. Biological flux of oxygen ($F_{bio} = F_a(O_2/Ar)$), against $F_a(^{17}O)$ (Equation 10) from the late freshet in June (blue triangles) and the low flow in August (red circles). Black star: bloom at station 5. Black diamond: seasonal transition at station 1 (Ambolikha site).

suggest that the high Δ(Ar) values in June are likely caused by the influence of snow melt (Figure S4 in Supporting Information S1).

$F_a(^{17}O)$ showed changes between June and August. Kolyma $F_a(^{17}O)$ was mostly negative in June (-5 ± 4 mmol m^{-2} d^{-1}), except at stations 13 and 19 (1 and 3 mmol m^{-2} d^{-1}, respectively). In contrast, $F_a(^{17}O)$ was >0 at all Ambolikha stations in June (6 ± 2 mmol m^{-2} d^{-1}), and August (average: 43 ± 27 mmol m^{-2} d^{-1}; Figure 7).

In Kolyma, positive $F_a(^{17}O)$ values were found at stations 5, 7 and 11 in August (at the confluence with tributaries, or associated with a bloom or pre-bloom (station 5); Figures 1 and 3). During the bloom at station 5, $F_a(^{17}O)$ was positive (141 mmol m^{-2} d^{-1}). This was the highest value, followed by neighboring station 4 (62 mmol m^{-2} d^{-1}). Combining $F_{adv}(^{17}O)$ with $F_a(^{17}O)$, allows calculating river-average gross oxygen productivity $G(^{17}O)$ (Table 3, row 12). Within the measurement uncertainty, $G(^{17}O)$ is zero for both rivers in June (Kolyma: -39 ± 37 mmol m^{-2} d^{-1}; Ambolikha: -4 ± 7 mmol m^{-2} d^{-1}). In August, both rivers had $G(^{17}O)$ value significantly above zero (Kolyma: 49 ± 39 mmol m^{-2} d^{-1}; Ambolikha: 88 ± 41 mmol m^{-2} d^{-1}, Table 3). Average negative $G(^{17}O)$ are shown in Table 3 and are assumed zero as they remain within their uncertainty range with the underlying productivity close to the detection limit.

3.6. Quantification of Carbon Flux Densities and the Contributions of Biotic and Abiotic Processes

In June, CO_2 emissions to the atmosphere, $F_a(CO_2)$, were about twice as high in the Ambolikha as in the Kolyma (57 ± 4 mmol m^{-2} d^{-1} vs. 27 ± 8 mmol m^{-2} d^{-1}, respectively; Table 3, row 1). Negative biological O_2 fluxes in Ambolikha ($F_a(O_2/Ar)$, $F_{adv}(O_2)$ and $F_{adv}(O_2/Ar)$; Table 3, rows 2, 3, 6 and 7), and the corresponding N values (Table 3, rows 10 and 11) indicate net respiration in both rivers, with no significant photosynthetic activity detected.

By August, average $F_a(CO_2)$ across both rivers declined by an order of magnitude (2 ± 4 mmol m^{-2} d^{-1} vs. 32 ± 14 mmol m^{-2} d^{-1} in June). In contrast to June, $N(O_2)$ and $N(O_2/Ar)$ became positive in both rivers (26–31 mmol m^{-2} d^{-1}; Table 3, rows 10 and 11), and gross oxygen productivity $G(^{17}O)$ was highest in the Ambolikha (88 ± 41 mmol m^{-2} d^{-1}), indicating a shift to net autotrophy. Several stations (4, 7, 16 and 25, as well as pre-bloom and bloom station 5) acted as small CO_2 sinks ($F_a(CO_2) = -1$ to -2 mmol m^{-2} d^{-1}) during the low-flow in August. Station 5 showed enhanced biological activity in August when $F_a(O_2/Ar) > F_a(O_2)$, compared

to June. Stations 4, 5 (pre- and at bloom event) and 11, were the only sites where $F_a(O_2/Ar)$ and $F_a(^{17}O)$ were positive throughout the study (Figure 7).

Respiration ($R = G(^{17}O) - N(O_2/Ar)$) remained large in both seasons in the Ambolikha (46 ± 22 mmol m^{-2} d^{-1} in June; 60 ± 43 mmol m^{-2} d^{-1} in August; Table 3, row 13), and during August R exceeded $F_a(CO_2)$ in both rivers as CO_2 fluxes approached equilibrium (Table 3, row 1). In June, R was close to $F_a(CO_2)$ only in the Ambolikha, while in the Kolyma $F_a(CO_2) > R$ (Table 3, rows 13 and 1). On average, the fluxes of CO_2 and O_2/Ar were an order of magnitude larger in June than August, confirming stronger emissions and heterotrophic activity during the late-freshet (Table 3, rows 1 and 3).

The gross oxygen productivity $G(^{17}O)$ in Ambolikha during August was nearly double (88 ± 41 mmol m^{-2} d^{-1}) than in Kolyma (49 ± 39 mmol m^{-2} d^{-1}; Table 3, row 12), reflecting the relevance of small tributaries to the ecosystem productivity in these river systems. During the August bloom at station 5, $G(^{17}O)$ peaked at 181 ± 79 mmol m^{-2} d^{-1}, twice the Ambolikha mean, underscoring the importance of localized bloom events.

3.7. Dissolved Organic Matter Signatures and Microbial Communities in Discrete Water Samples

Seasonal transitions and tributary inflows strongly shape the molecular composition of dissolved organic matter (DOM) and the structure of microbial communities in permafrost-affected rivers. Integrating high-resolution mass spectrometry with multivariate analyses, we identified consistent seasonal clusters and site-specific signatures reflecting hydrological and ecological dynamics (Figure 8 and Figures S5–S10 in Supporting Information S1).

As large storage of organic carbon is locked in permafrost, quantitative differences among the discrete samples from the late-freshet and low-flow periods can be associated with qualitative differences in the DOM profile. This is illustrated by the hierarchical cluster analysis (HCA, Figure 8a) and principal coordinate analysis (PCoA, Figure 8b). High-resolution mass spectrometry identified 1,818 DOM molecular formulas across all samples. Cluster analysis and PCoA separated the data set into five coherent groups: three associated with the late freshet in June (clusters A-I, A-II, A-III) and two with the low-flow conditions in August (clusters B-I, B-II; Figures 8a and 8b). These seasonal shifts were consistent with cross-validation in discriminant analysis (Table S2 in Supporting Information S1).

Although the relative abundance of identified compounds varied between June and August, their elemental composition remained similar (Figure S5 in Supporting Information S1). Most DOM consisted of C, H and O atoms (86% in June, 91% in August); while heteroatom-containing molecules comprised <14% of the total. Significant seasonal compounds (sSC, Supplement B in Supporting Information S1) occurred primarily within the lignin-like class (Figure S5 in Supporting Information S1) and distinct clusters represented seasonal changes in the Kolyma (clusters A-III vs. B-I; Figure 8b). Moreover, significant differences between rivers were observed, as the riverine compounds (sRC, Supplement B in Supporting Information S1) formed separate clusters for Ambolikha and Kolyma (clusters A-II vs. A-III (Figure 8) and B-I versus B-II (Figure S6 in Supporting Information S1)).

Stations 7, 9, and 11 in June, located at tributary confluences (Figure 1), displayed distinct DOM signatures that set them apart from other sites (cluster A-I; Figures 8a and 8b). These unique DOM signatures likely reflect stronger contributions from tributaries transporting meltwater and DOM from thawing permafrost. After subtracting features shared with Kolyma freshet samples (A-III), 271 candidate molecules remained (Figure S10 in Supporting Information S1), 92 of which match previously reported as permafrost-thaw signatures (Spencer et al., 2015; Figure S10 in Supporting Information S1, Appendix A3).

The DOM PCoA analysis shows that Ambolikha stations 1–4 also form a cluster in June (Figure 8a), consistent with the PCA of water properties at the station level (Figure 4a). During the low-flow period, Kolyma station 5 clustered with Ambolikha samples (B-I), confirming the influence of inflowing rivers (Figure S5 in Supporting Information S1). At station 5, the core set of compounds detected before and during the bloom shared ~40% of all features (724 compounds). However, the bloom altered ~32% of molecular features within three days (Figure S7 in Supporting Information S1): 125 pre-bloom compounds persisted, while 110 significant bloom-specific compounds (sBC; Supplement B in Supporting Information S1) emerged, mainly within the CHO class along with some sulfur-containing molecules (Figure S7 in Supporting Information S1).

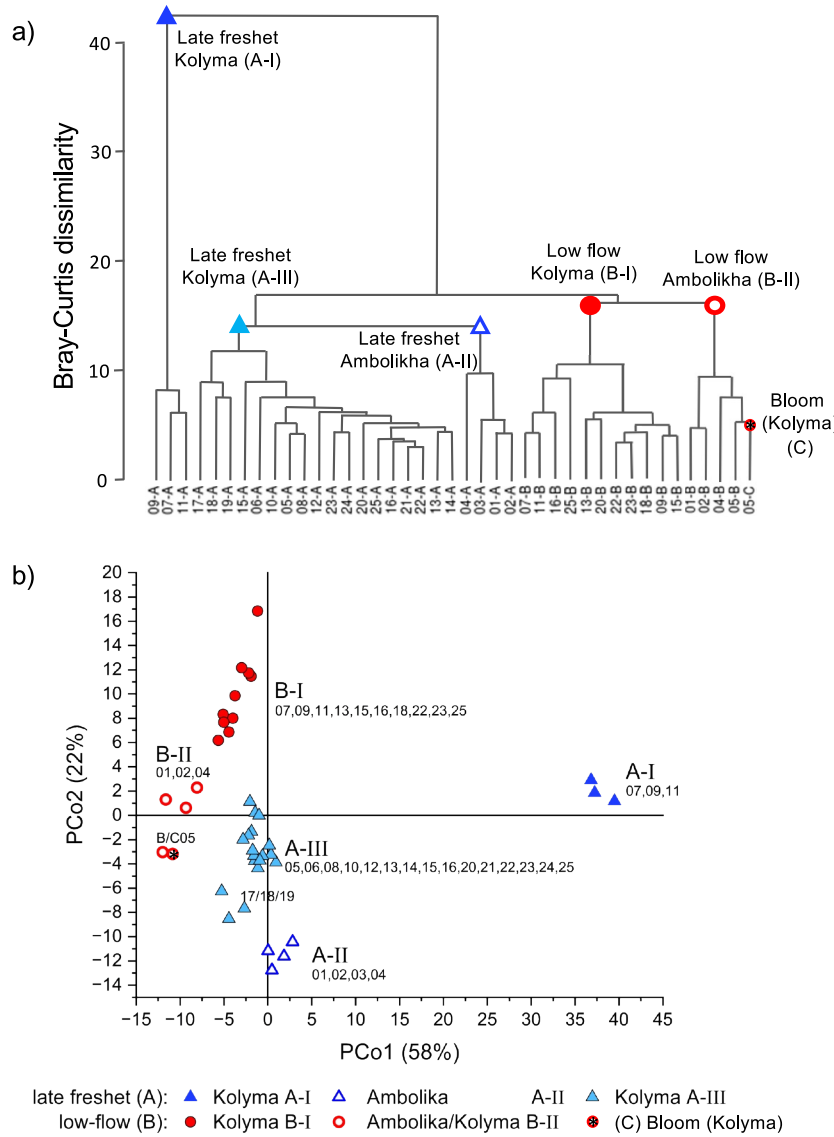

Figure 8. (a) Hierarchical Cluster Analysis (HCA) confirms the sub-groupings indicated by Roman numerals in panel (a). The same color scheme is used in both panels. (b) Principal Coordinate Analysis (PCoA) reveals patterns in dissolved organic matter (DOM) composition and identifies distinct groupings: late freshet in June (Group A), low-flow conditions in August (Group B). Blue triangles represent late freshet samples (sub-groups A I–III), while red circles indicate low-flow samples (sub-groups B I–II), including the bloom sample (C). Labeling was accomplished according to the cluster analysis in panel (a).

Microbial communities mirrored DOM and hydrochemical patterns. Community structure differed significantly between Ambolikha and Kolyma (Figure S8a in Supporting Information S1, permanova: $F = 18$, $p < 0.001$, $R^2 = 0.13$) and between June and August (Figure S8 in Supporting Information S1; $F = 23$, $p < 0.001$, $R^2 = 0.17$). The bloom at station 5 was dominated by the diatom *Melosira* sp. (possibly *M. varians*; Bacillariophyceae; Figures S2c, S2d, and S9 in Supporting Information S1) and cyanobacteria (*Nostocaceae*, *Cyanobiaceae*, and *Microcystaceae*), with photosynthetic bacteria reaching ~40% of the total community (Supplement F in Supporting Information S1). Downstream, phototroph abundance declined to ~20%, while upstream at station 1 it was ~10% (Figure S8b in Supporting Information S1), indicating the localized impact of the bloom on microbial assemblages, with potential consequences for nutrient cycling and food web interactions. Along the main stem of the Kolyma, the transect showed greater variance in beta-diversity than the Ambolikha, forming putative clusters along a sample gradient unrelated to the direction of water flow, and instead thought to be influenced by the

proximity of tributary inflows. Overall, DOM composition and clustering patterns showed strong seasonal variability, driven by tributary inflows, permafrost-derived inputs and bloom events. These shifts were accompanied by marked changes in microbial community structure.

4. Discussion

4.1. Seasonal Variations in Hydraulic Properties Control Changes in Chemical and Biological Variables

The open-water period in Arctic Rivers is characterized by warmer temperatures and more daylight, expected to be the most biologically active period. It lasts ~150 days and is bracketed by the ice-covered, dark and lowest annual flow season (November–April; Holmes et al., 2012).

In this study, we characterized biological productivity in the Kolyma and Ambolikha rivers during the open water period in 2019. In 2019, the Kolyma was ice-free for 146 days (20 May–12 October), with discharge peaking on 31 May (27.7×10^3 m^3 s^{-1}; Shiklomanov et al., 2020; Figure S1 in Supporting Information S1). Our sampling in June after the peak discharge (late-freshet) and August (low-flow) captured strong seasonal contrast in water properties: warmer, oxygen-rich and lower conductivity waters in June, and more conductive waters in August due to reduced dilution and greater solute inputs. During the late freshet period, the elevated discharge transports substances and freshwater from land and headwater, providing a distinctive signal that spreads downstream, affecting smaller and larger tributaries. In August, the discharge in the main Kolyma stem receded, and the base water level dominated across the watershed; thus, a more homogeneous spatial distribution of properties is encountered between streams and the channel. Figure 9 summarizes our observations, illustrating the seasonal transition from the late-freshet to low-flow conditions, highlighting changes in water level, O_2 dynamics, DOM composition, and microbial communities at tributary-influenced stations (i.e., 4, 5 and 11).

More depleted water isotope $\delta(^{18}O, H_2O)$ in June confirmed snowmelt compared to August (Figure 6), and DOM fingerprints were also different in the seasons (Figure 8). These results are consistent with previous findings in Ambolikha (Castro-Morales, Canning, Körtzinger, et al., 2022). The present study adds spatial resolution along the Kolyma.

CO_2 was consistently supersaturated in June and August, but its source likely shifted from terrestrial inputs during freshet to in situ respiration during low-flow due to varying hydraulic conditions (Hotchkiss et al., 2015). Smaller tributaries like Ambolikha, emitted more CO_2 (57 ± 4 mmol m^{-2} d^{-1}) per unit area than the Kolyma (27 ± 8 mmol m^{-2} d^{-1}) during June, likely due to closer soil connections. In August, CO_2 emissions declined markedly (2 ± 4 mmol m^{-2} d^{-1}) in both rivers, reflecting reduced turbulence and water flow (Table 3).

O_2 dynamics showed a similar transition to that of CO_2, and together with O_2/Ar ratios, the predominant biological or physical processes influencing O_2 cycling were identified. In June, both rivers had high turbidity (Table 1), limiting the light penetration in the water column. Supersaturated $\Delta(O_2)$ and Δ(Ar) (Figure S4 in Supporting Information S1) but negative $\Delta(O_2/Ar)$ (Figure 5) in the Kolyma, indicated physical drivers (warming, air injection from ice melt, and turbulence). High Δ(Ar) in the Kolyma is likely a result of a sudden warming without sufficient time for the gas concentration to equilibrate, confirming the influence of physical processes.

The Ambolikha however, was not influenced by turbulent flow and showed biological O_2 drawdown under turbid, light-limited conditions ($\Delta(O_2)$ around −32%; Figures 3 and 5).

Enhanced biological productivity during the melt period has been observed in Arctic inland waters such as tundra ponds, where nutrient pulses stimulate phytoplankton growth (Dokulil & Qian, 2021; Miller, 2013). In contrast, high discharge in large rivers typically suppresses phytoplankton growth and settling because of turbidity, particle resuspension, and freshwater dilution (e.g., Descy et al., 2017; Dokulil, 2015; Dokulil & Qian, 2021). Our results from the Kolyma and Ambolikha confirmed this pattern as high flows limited phytoplankton settlement through dilution, downstream transport, and short residence times (Allan & Castillo, 2007).

By August, reduced flow, lower turbulence, and longer water residence times in the Kolyma and Ambolikha led to more lentic conditions, typical of seasonal transitions in rivers worldwide (Collins et al., 2024; Schulz et l., 2023). These conditions increased exposure of organic carbon to mineralization, enhancing decomposition rates (Catalán et al., 2016). Our results show that biological activity dominated during low flow conditions, with $\Delta(O_2/Ar)$ up to 6% at tributary confluences (stations 4, 5 and 11), supporting localized phytoplankton growth. $\Delta(O_2)$ and $\Delta(O_2/Ar)$ shifted toward saturation at other stations (Figures 1 and 5), indicating potential for phytoplankton bloom

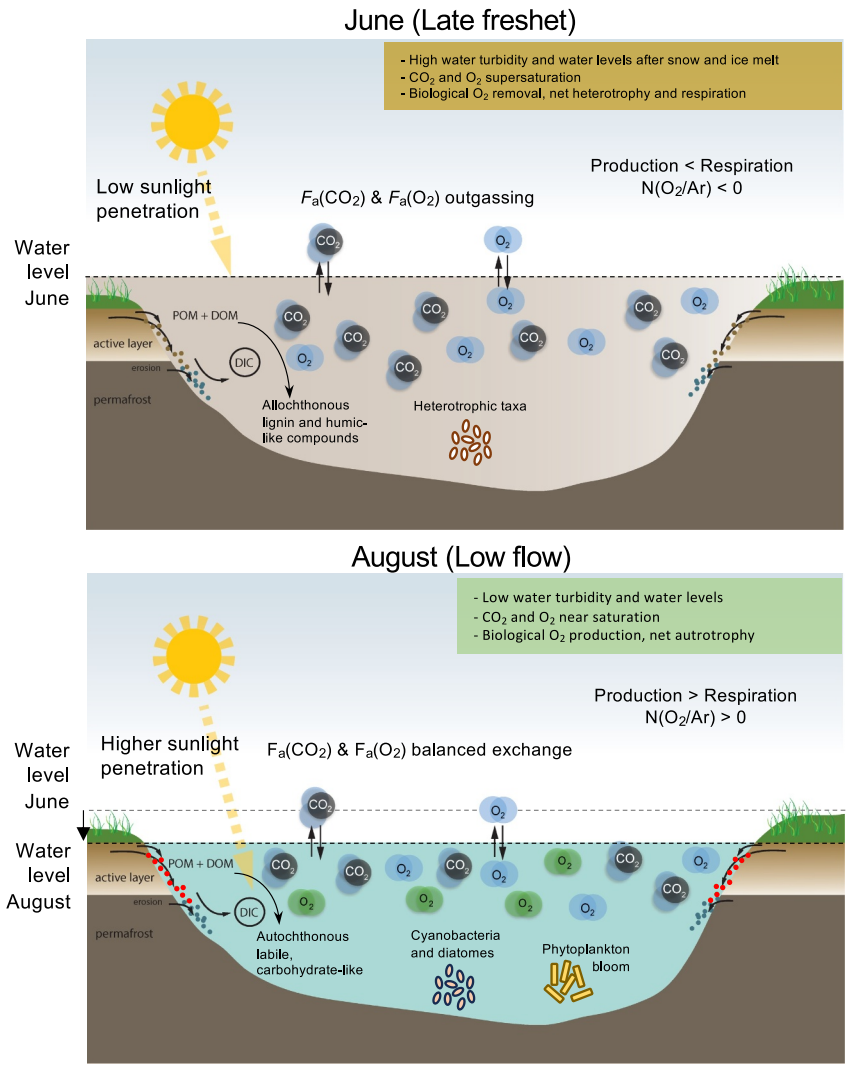

Figure 9. Schematic representation of the seasonal change in stations 4, 5 and 11 in Kolyma and Ambolikha rivers. *Top:* Late-freshet (June) conditions with high water levels and turbidity limiting the light penetrations in surface waters. Elevated $F_a(CO_2)$ and $F_a(O_2)$ with dominant abiotic O_2 (blue O_2 molecules) and net heterotrophy ($N(O_2/Ar) < 0$), and distinctive organic matter and microbiome. *Bottom:* Low-flow (August) conditions with lower water levels and turbidity, allowing more light penetration and biological production of O_2 (green O_2 molecules) (N(O2/Ar) > 0) in stations 4, 5 and 11, lead to a phytoplankton bloom in station 5. $F_a(CO_2)$ and $F_a(O_2)$ are near equilibrium with the atmosphere. From June to August, Arctic rivers shifted from allochthonous, heterotroph-dominated systems to autochthonous, bloom-forming communities fueled by photosynthetic microbes and labile DOM.

development if low turbidity and slow flows persisted. Hydropower regulation with a dam near Kolymsk-1, further reduces flow in the Kolyma during low discharge (Gabyshev & Gabysheva, 2013).

Despite short Arctic growing seasons due to low temperatures, nutrient limitation and reduced sunlight (Hurry et al., 2002), phytoplankton blooms in Arctic rivers can develop from the assimilation of permafrost-derived carbon by microorganisms (Vishnivetskaya et al., 2020). Ultimately, the success of phytoplankton populations to establish and grow in boreal rivers depends on their capacity to withstand reduced light availability and turbulent conditions (Burrows et al., 2021; Descy et al., 2017). In the lower Kolyma, slower flow allows different phytoplankton community structures than in more dynamic headwaters (Gabyshev & Gabysheva, 2013). The August bloom at station 5 developed in a slow-flowing part of the lower Kolyma, near the confluence with the Panthelika tributary, where dissolved O_2 concentrations increased downstream.

The relative abundances of putative photosynthetic microorganisms strongly reflect the patterns in biological productivity. Cyanobacteria, nearly absent during the freshet, increased to ~40% of the community in the bloom, forming dense green mats (Figure S2c in Supporting Information S1). Photosynthetic microorganisms can be released during permafrost thaw and thrive in low-flowing environments (Vishnivetskaya et al., 2020). Microscopic analysis identified a diatom of the genus *Melosira* sp. (Bacilliariophyceae, Melosiraceae; Figure S9 in Supporting Information S1), tolerant of salinities from 0.5 to 30 (Pratiwi et al., 2018; Suryaningtyas et al., 2022) and previously reported in Arctic waters (Holger, 1997; Potapova, 2014). While *Melosira varians* has not been previously reported in the Kolyma waters (compared to rivers and lakes of North America; Potapova, 2019), it has been detected in Kolyma sediment cores (Wetterich et al., 2017, 2018). Indeed, the class *Bacilliariophyceae* dominated density and biomass in the Kolyma by up to 71% (Gabyshev & Gabysheva, 2013). Similar patterns are observed in the Lena River, where diatoms and picocyanobacterial biomass dominate lower and delta regions due to lower turbidity and higher light availability (Sorokin & Sorokin, 1996). However, microscopy alone cannot quantify the actual contribution of these organisms to productivity. Their role is inferred from O_2 fluxes, $\Delta(O_2/Ar)$, and isotopic ratios, integrating photosynthetic and respiratory rates during the bloom.

The presence of the bloom also coincides with shifts in the DOM composition with season, location and proximity to tributaries, emphasizing its role in Arctic river biogeochemistry. DOM contains protein-like, humic-like, and carbohydrate components essential for nutrient recycling, microbial energy transfer, and primary productivity (Ma et al., 2021; Mackay et al., 2020; Zhang et al., 2009). DOM in Arctic rivers originates from both allochthonous material from runoff and permafrost thaw, and autochthonous production from secretion and decomposition of aquatic plants, algae, and microbes (Adamczuk, 2021; Spencer et al., 2015; Zhang et al., 2009). Autochthonous DOM, rich in labile carbohydrates, fuels microbial processes and primary productivity via nutrient recycling, whereas allochthonous DOM provides a reservoir of terrestrial carbon (Bao et al., 2023; Yang et al., 2020), particularly during blooms (Figure S7 in Supporting Information S1). Permafrost thaw can further supply nutrients and DOM that alter microbial activity and accelerate DOM transformation and degradation. Thus, the ratio of allochthonous to autochthonous organic matter regulates nutrient cycling, carbon dynamics, and food web structure, though distinguishing its origin remains challenging (Spencer et al., 2015).

In this study, tributaries influenced by permafrost thaw contributed allochthonous DOM detectable at stations 7, 9, and 11. Molecular signatures matched previously reported markers of permafrost-derived carbon, including lignins, in Arctic rivers (Spencer et al., 2015; Figure S10 in Supporting Information S1). Lignins were prominent in our van Krevelen plots (Figures S5–S7 in Supporting Information S1). This group of compounds is a major terrestrial plant-derived polymer resistant to decomposition, and is one of the major constituents of organic matter in permafrost. Thus, lignins are a reliable indicator of terrestrial (allochthonous) DOM input, making possible the distinction from autochthonous sources (plant, algal, or microbial sources). Previous findings with stable carbon isotopes further support the seasonal changes: during the freshet, most DOC in the Kolyma River is allochthonous as indicated by its $\delta^{13}C$ signal (Keskitalo et al., 2022), while in low-flow conditions, the DOC becomes more ^{13}C-depleted suggesting a larger autochthonous contribution. Although terrestrial material remains the dominant DOC source, assimilation by algae during low-flow conditions can transform it into autochthonous biomass. For instance, sulfur-containing DOM features may serve as additional biomarkers of microbial activity during seasonal transitions (Schmidt, 1988).

Overall, these observations show how flow reduction, lentic conditions, and tributary inputs promote blooms, while DOM composition both reflects and supports microbial activity, linking riverine carbon sources to primary productivity and nutrient cycling in Arctic rivers (Figure 9).

4.2. Environmental Factors Influencing Biological Productivity

Beyond discharge, turbulence, and turbidity (limiting light availability), other factors such as temperature and nutrient availability influence phytoplankton populations (Allan & Castillo, 2007; Myrstener et al., 2018). In the Arctic Ocean, productivity is mainly controlled by nutrient supply and light (Codispoti et al., 2013; Matrai et al., 2013; Myrstener et al., 2022; Terhaar et al., 2021; Yun et al., 2016), while in rivers like the Donan in Indonesia, nitrate, light, salinity, and $c(O_2)$ influence phytoplankton abundance (Pratiwi et al., 2018). In our study, $c(NO_x^-)$ was communicated by $c(NO_3^-)$ (90% in June, 86% in August), followed by $c(NO_2^-)$ (10% in June, 14% in August). Bloom nitrate (1.1 μmol L^{-1}) was less than half of pre-bloom levels (2.5 μmol L^{-1}), indicating consumption during the bloom. In the Arctic Ocean, nitrate is often assimilated by heterotrophic bacteria, while

phytoplankton biomass is low (c(Chl a) < 2 μg L^{-1}) and relies on urea (Fouilland et al., 2007). In the Kolyma, nitrate assimilation appears to support phytoplankton growth. Nonetheless, hydrologic conditions and turbidity remain the driving mechanisms of phytoplankton settlement and bloom development, though lateral nutrient inputs from permafrost thaw along the river continuum can further influence aquatic metabolism (Francis et al., 2023). Thus, the temporal variations in water properties in both rivers were possibly driven by the decline of discharge and the air temperature decrease between June and August.

Tributaries also contribute to productivity by seeding phytoplankton populations. The Omolon River, the largest Kolyma tributary, strongly influences downstream phytoplankton populations (Gabyshev & Gabysheva, 2013). The outlet of the Omolon is 40 km upstream from station 25 on the left bank of the channel and near the Kolymsk-1 gauge station (Figure 1). Although we did not sample the Omolon confluence, the bloom at station 5 near the Panthelika/Ambolikha confluence (Figure 1), shows tributary influence, supported by DOM profiles clustering with Ambolikha stations 1 to 4 (Figure 8 and Figure S3 in Supporting Information S1). High fDOM concentrations can be due to a higher input from headwaters or lateral transfers and were expected to be found in turbid waters.

Vertical profiles during the bloom at station 5 revealed subsurface c(Chl a) concentrations at 0.25 and 0.48 m depth, three times higher than the waters above and below (Figure S2 in Supporting Information S1). Such subsurface c(Chl a) maxima are common in stratified Arctic waters and develop after nutrient depletion due to photoacclimation in regions of high light incidence; however, they might not coincide with maximum phytoplankton biomass (Brown et al., 2015; Cullen, 2015). Subsurface c(Chl a) and $c(O_2)$ maxima can also be decoupled depending on water column structure (Rollo et al., 2020). At station 5, F_{bio} increased to 6 mmol m^{-2} d^{-1} during the bloom, compared with −25.3 mmol m^{-2} d^{-1} in June and 1 mmol m^{-2} d^{-1} just 3 days before the bloom.

4.3. Method Robustness and Limitations

Arctic rivers are naturally low in O_2 and high in CO_2. The O_2/Ar measurements confirmed the prevalence of net heterotrophy even when O_2 was supersaturated, with this supersaturation attributed to abiotic processes such as meltwater input (Figure 5). Combined measurements of gross productivity G based on O_2 triple isotopologues (G(^{17}O)) and net productivity N based on O_2/Ar ($N(O_2/Ar)$) demonstrated the coexistence of gross carbon uptake (gross production) and net heterotrophy. By including the advective oxygen fluxes in a robust mass balance, in June there is an overall loss of oxygen from upstream to downstream waters, whereas in August there is an apparent gain as the river flow is slower and more opportunities for phytoplankton communities to settle downstream.

The biological O_2 supersaturation $\Delta(O_2/Ar)$ not only served as a valuable tracer for biologically produced oxygen but also as an indicator of water sources. In June, we observed a significant Ar supersaturation $\Delta(Ar) = 26 \pm 4\%$. This can be largely explained by rapid warming without sufficient time for the gas concentrations to equilibrate, but may also reflect contributions from air injection from melting ice, in line with high N_2/Ar ratios in permafrost ice wedges (Park et al., 2022). High Δ(Ar) values (up to 3%) in Canadian Basin surface waters were attributed to the release of Ar-enriched bubbles trapped in sea ice (Eveleth et al., 2014).

The average negative $G(^{17}O)$ values shown in Table 3 are considered here as zero because the values remain within the uncertainty. To avoid negative values, the measurement model could be refined in the future. For example, recent measurements have shown γ_R values as low as 0.499 for the ratio of $^{17}O/^{16}O$ to $^{18}O/^{16}O$ respiratory fractionation during abiotic photochemical DOC oxidation (Sutherland et al., 2022). A γ_R value below 0.5179 (used in this study) would bring the calculated $G(^{17}O)$ values closer to 0. However, in our low-productivity system even such extreme and unlikely variations in the parameters would not significantly alter the results because the samples contain very little photosynthetic O_2.

4.4. Comparison to Productivity Estimates for Other Arctic Rivers

Aquatic productivity can be quantified using $^{13}C/^{12}C$ ratios of DOC, radiocarbon (^{14}C) or $H_2{}^{18}O$ assimilation during photosynthesis, or diel $c(O_2)$ variations (Regaudie-de-Gioux et al., 2014). Though methods often yield different results and require cautious comparison of results. While estimates for Arctic rivers are scarce, Arctic

Ocean studies show high spring productivity in marginal seas and strong river influence (e.g., Codispoti et al., 2013; Matrai et al., 2013; Terhaar et al., 2021; Ulfsbo et al., 2014).

Reported approaches on productivity in Arctic rivers include phytoplankton biomass (Sorokin & Sorokin, 1996), dissolved O_2 (Huryn et al., 2014), and $\delta(^{13}C_{DIC})$, CO_2 and O_2 measurements (Rocher-Ros et al., 2019, 2020). For example, ^{14}C assimilation in the Lena River averaged 0.18 g m^{-2} d^{-1} (mass fluxes in this section are given as C equivalents), peaking at 1.2 g m^{-2} d^{-1} at the mouth. In a small shallow and warmer slow flowing stream of the Ivishak Spring (Alaska; average discharge of 0.136 m^3 s^{-1}), July gross productivity estimated from $c(O_2)$ variations was mostly driven by light, and yielded 4.4 g m^{-2} d^{-1}, with respiration twice as high (8.7 g m^{-2} d^{-1}; Huryn et al., 2014). Ambolikha productivity ($G(^{17}O) = 88 \pm 41$ mmol m^{-2} d^{-1}; or 1.1 ± 0.5 g m^{-2} d^{-1}, for a 1:1 ratio of O_2:CO_2) in August was comparable to the Lena River maximum but four times lower than in the Ivishak Spring.

Isotopic tracers ($^{14}C/^{12}C$ and $^{13}C/^{12}C$ ratios of DOC and POC) in the Kolyma reveal that summer POC was dominated by $\delta(^{13}C_{POC})$, consistent with in-stream productivity fueled by terrigenous CO_2 (Bröder et al., 2020; Keskitalo et al., 2022). Continuous $c(O_2)$ and $c(CO_2)$ measurements in northern Sweden streams showed net heterotrophy ($N < 0$), with a net ecosystem productivity (NEP) = -1.7 g m^{-2} d^{-1} from the late freshet (June) to autumn (September) of 2015 and 2016 (Rocher-Ros et al., 2019). Similarly, the Ambolikha and Kolyma were net heterotrophic in June, with $N(O_2/Ar)$ of -0.6 and -0.4 g m^{-2} d^{-1} (-50 and -37 mmol m^{-2} d^{-1}; Table 3, row 11), consistent with Alaskan rivers (Rocher-Ros et al., 2020). In June, respiration accounted for 81% of CO_2 flux ($F_a(CO_2)$) in the Ambolikha and exceeded $F_a(CO_2)$ considerably in August for both rivers (Table 3). The average June and August $F_a(CO_2) = 22 \pm 18$ mmol m^{-2} d^{-1} for both rivers was equivalent to 12 ± 23% of $G(^{17}O)$ during the bloom event (181 ± 79 mmol m^{-2} d^{-1}), indicating strong metabolic influence on CO_2 emissions and supporting conclusions of Rocher-Ros et al. (2020).

The CO_2 concentration is affected by biological and physical processes, such as photochemical oxidation of organic carbon, organic matter degradation by bacteria, respiration, lateral inputs of surface or groundwaters, gas exchange and vertical mixing (when the river is stratified). Some of these processes contribute more than respiration: Photochemical oxidation was estimated to contribute about one-third to CO_2 emissions (Cory et al., 2014), with the remainder comprising CO_2 from soil respiration and groundwater inflow and a minor (3%) contribution from in-stream respiration (Winterdahl et al., 2016). 28% of CO_2 emissions from US streams and rivers are estimated to be due to ecosystem respiration, with emissions increasing with channel size (Hotchkiss et al., 2015). This is close to the estimated 30% contribution of in-stream metabolism to spring and summer CO_2 emissions from UK streams (Rovelli et al., 2022). High turbulence in the river, especially in spring, promotes CO_2 emission.

In line with others (Rocher-Ros et al., 2019, 2020), we show that respiration is high in Arctic rivers, particularly in small tributaries such as the Ambolikha, amounting to 81% of CO_2 emissions in June, and up to 70 times higher than the CO_2 emissions in August. In the Kolyma river, R in August is six times $F_a(CO_2)$. Our results also show a shift in the metabolic balance from June late freshet to August low flow period, as well as the influence of smaller tributaries. While net heterotrophy dominated in June ($N < 0$) in both rivers, net productivity dominated in August ($N > 0$), with higher $F_a(O_2/Ar)$ at sites close to tributaries (stations 4, 5 and 11). The intermittent appearance of blooms during the low-flow period seemed to be spatially confined to river sections with suitable hydraulic conditions, available nutrients and light. Blooms in Arctic rivers are likely sporadic events during low-flow periods that last only a few months every year. Thus, sporadic bloom events are unlikely to currently turn Arctic Rivers into net carbon sinks over a complete annual cycle. However, further studies are warranted as this might change in the future warming climate.

4.5. Perspectives for a Changing Climate

The observed shift to earlier freshets and later freeze-up in Arctic rivers (Holmes et al., 2021a), will lead to longer open water periods, which will affect these ecosystems. Water retention time controls organic carbon decomposition in inland waters (Catalán et al., 2016), and according to satellite imagery analysis over the last 50 years, Arctic rivers are slowing down at a mean rate of 3.7% per year in response to climate warming and expansion of shrubs in river banks, which in turn limits the overland water flow (Ielpi et al., 2023). The discharge of Arctic rivers is changing over time, but it is unclear if this is due to increased precipitation in winter, changing timing of snowfall, or snow accumulation (Holmes et al., 2021a). As longer open water seasons in response to early melt is

predicted with climate change (Francis et al., 2023; Holmes et al., 2021b), and the river flow slows, a summer low-flow characteristic (lotic to lentic) will prevail after the freshet period and enable the environmental conditions for the growth and settlement of primary producers.

An increase in DOC export as a result of increasing discharge has recently been documented (Clark et al., 2023), which might lead to an increase of in-stream DOM processing and CO_2 availability (Hotchkiss et al., 2015). However, the increased DOC export can also expand areas with light limitation.

We showed that for Kolyma low-flow conditions, availability of nutrients and light provided a suitable environment for developing a phytoplankton bloom at the confluence with the Pantheleika/Ambolikha Rivers (Figure 9). This agrees with analyses of US rivers, where light and flow regimes are drivers of gross primary productivity and ecosystem respiration (Bernhardt et al., 2022). Thus, the river conditions during low-flow (Figure 9, bottom) may be enhanced under climate warming.

Radiocarbon (^{14}C) measurements in tundra ponds of Alaska showed an increase in net primary productivity in recent years compared to 40 years earlier, indicating a potential shift of these ecosystems from sources to annual net carbon sinks (Miller, 2013). A consistent decline in CO_2 emissions over a period of 23 years was observed in lakes in the sub-Arctic tundra region of Nunavut, Canada (Brothers et al., 2021), and these observations might support a metabolic shift, specifically in primary production, in response of climate warming in Arctic freshwater ecosystems.

Organic matter and nutrients from thawing active layers may enhance carbon uptake in Arctic rivers and streams during more extended low-flow conditions. The development and persistence of blooms can then become more common during the open water season, enhancing biological carbon uptake and respiration. This raises the question: Are Arctic rivers shifting towards higher productivity in response to climate change?

The contribution of permafrost carbon released after thaw to biological productivity and organic carbon mineralization in the river is still unclear. The CO_2 excess in Arctic rivers is mostly fueled by the mineralization of terrigenous material, and lateral inputs from soil microbial and root respiration in and around small streams (Ward et al., 2017; Wild et al., 2019). However, DOC composition in Arctic rivers is dominated by recent primary production and contains only 12% of permafrost organic carbon (Wild et al., 2019), with the remainder in the particulate pool (Keskitalo et al., 2022; Wild et al., 2019). In addition, most CO_2 emissions originate from the in situ oxidation of recent carbon (Dean et al., 2020), particularly in large rivers. Therefore, it is likely that productivity and autochthonous organic matter production are currently sustained by the uptake of recycled allochthonous carbon, which contains only a partial contribution from permafrost sources.

5. Conclusion

This study of Arctic rivers highlights the interplay between hydrology, biological productivity, and gas dynamics under a warming climate. Seasonal contrasts were strong: during the late freshet, high turbulence and dilution promoted net heterotrophy, with respiration and CO_2 release dominating, whereas low-flow conditions in August favored net autotrophy, with enhanced gross oxygen production at localized phytoplankton blooms. Slower flows and increased light penetration at tributary confluences supported phytoplankton settlement and growth, while microbial communities shifted from low abundances of photosynthetic bacteria in June to up to 40% of the community during blooms. Similarly, DOM composition reflected both seasonal hydrology and tributary inputs, that is, freshet waters enriched in lignin-like allochthonous compounds and low-flow waters with more labile autochthonous components. Despite in-river productivity pulses, the contribution of permafrost carbon to new aquatic productivity remains unclear. Most CO_2 excess in Arctic rivers derives from the mineralization of recent terrestrial carbon, with only limited contributions from permafrost sources. Overall, autochthonous production appears primarily supported by recycled allochthonous DOM, highlighting the importance of tributary inputs, microbial dynamics, and hydrological shifts shaping the carbon balance of Arctic rivers. Future research should aim to quantify the contributions of allochthonous and autochthnonous carbon to aquatic productivity, and evaluate their impact on carbon cycling and greenhouse gas dynamics in Arctic rivers.

Conflict of Interest

The authors declare no conflicts of interest relevant to this study.

Data Availability Statement

The hydrochemical continuous and discrete data presented in this study are available at the Zenodo EU repository via https://doi.org/10.5281/zenodo.15229557 under the license Creative Commons Attribution 4.0 Internations (Castro-Morales, 2025).

Acknowledgments

This work was conceived and developed for the project PROPERAQUA funded by the Deutsche Forschungsgemeinschaft (DFG, German Research Foundation) 396657413 led by K.C-M. The EU project C-CASCADES ITN (643052) funded A.C. and A.K., as well as the MOSES program of the Helmholtz Association. T.W. and S.R. were funded by the DFG in the framework of the priority program (SPP 1158) "Antarctic Research with comparative investigations in Arctic ice areas" (424256657). M.G. and O.K. were supported through funding by the EU projects INTAROS (727890) and Nunataryuk (773421), and the German Ministry of Education and Research (KoPf project, Grant 03F0764D). K.K. and W.A.O were supported by the Collaborative Research Centre 1076 AquaDiva (CRC AquaDiva) funded by DFG (218627073). J.K. was supported from the UK Research and Innovation (UKRI) Grant 10040851, linked to Grant 101056921 of the European Union's Horizon EUROPE research and innovation program. The analysis of O_2/Ar and triple oxygen isotopes in river samples were done at the Stable Isotope Laboratory at UEA, UK, under contractual service agreement with FSU Jena. The authors thank the personnel of the Northeast Scientific Station and Pleistocene Park in Chersky for their valuable assistance during the field work, particularly to Sergey Zimov and Galina Zimova. Thanks to Heiko Moosen and Heike Geilmann for the analysis of water stable isotope at the MPI-BGC IsoLab, and to Robert Lehmann for the DOC analysis at the FSU Jena. Special thanks to Kirsi Keskitalo, Juri Palmtag and Jan Strauss, for their valuable support on the field and the transportation of water samples to Germany during the global COVID-19 pandemic. The authors thank the constructive and thorough comments from two anonymous reviewers that contributed to improve this work. Open Access funding enabled and organized by Projekt DEAL.

References

Abril, G., Bouillon, S., Darchambeau, F., Teodoru, C. R., Marwick, T. R., Tamooh, F., et al. (2015). Technical note: Large overestimation of pCO_2 calculated from pH and alkalinity in acidic, organic-rich freshwaters. *Biogeosciences*, *12*(1), 67–78. https://doi.org/10.5194/bg-12-67-2015

Adamczuk, M. (2021). Do experimental conditions bias plankton responses to increased concentration of dissolved organic matter (DOM)? A meta analytical synthesis of the published results. *Science of the Total Environment*, *787*, 147590. https://doi.org/10.1016/j.scitotenv.2021.147590

Allan, J. D., & Castillo, M. M. (2007). *Stream ecology structure and function of running waters* (2nd ed.). Springer.

Amorocho, J., & Devries, J. J. (1980). A new evaluation of the wind stress coefficient over water surfaces. *Journal of Geophysical Research*, *85*(C1), 433–442. https://doi.org/10.1029/JC085iC01p00433

Aron, P. G., Levin, N. E., Beverly, E. J., Huth, T. E., Passey, B. H., Pelletier, E. M., et al. (2021). Triple oxygen isotopes in the water cycle. *Chemical Geology*, *565*, 120026. https://doi.org/10.1016/j.chemgeo.2020.120026

Ayala-Borda, P., Bogard, M. J., Grosbois, G., Prèskienis, V., Culp, J. M., Power, M., & Rautio, M. (2024). Dominance of net autotrophy in arid landscape low relief polar lakes, Nunavut, Canada. *Global Change Biology*, *30*(2), e17193. https://doi.org/10.1111/gcb.17193

Bao, Y., Huang, T., Ning, C., Sun, T., Tao, P., Wang, J., & Sun, Q. (2023). Changes of DOM and its correlation with internal nutrient release during cyanobacterial growth and decline in Lake Chaohu, China. *Journal of Environmental Sciences*, *124*, 769–781. https://doi.org/10.1016/j.jes.2022.02.019

Barbato, R. A., Jones, R. M., Douglas, T. A., Doherty, S. J., Messan, K., Foley, K. L., et al. (2022). Not all permafrost microbiomes are created equal: Influence of permafrost thaw on the soil microbiome in a laboratory incubation study. *Soil Biology and Biochemistry*, *167*, 108605. https://doi.org/10.1016/j.soilbio.2022.108605

Benson, B. B., Krause, D., & Peterson, M. A. (1979). The solubility and isotopic fractionation of gases in dilute aqueous solution, I. Oxygen. *Journal of Solution Chemistry*, *8*, 655–690. https://doi.org/10.1007/bg01033696

Berggren, M., Lapierre, J.-F., & del Giorgio, P. A. (2012). Magnitude and regulation of bacterioplankton respiratory quotient across freshwater environmental gradients. *The ISME Journal*, *6*(5), 984–993. https://doi.org/10.1038/ismej.2011.157

Bernhardt, E. S., Savoy, P., Vlah, M. J., Appling, A. P., Koenig, L. E., Hall, R. O., Jr., et al. (2022). Light and flow regime regulate the metabolism of rivers. *Proceedings of the National Academy of Sciences of the United States of America*, *119*(8), e2121976119. https://doi.org/10.1073/pnas.2121976119

Bogard, J. M., Vachon, D., St-Gelais, N. F., & del Giorgio, P. A. (2017). Using oxygen stable isotopes to quantify ecosystem metabolism in northern lakes. *Biogeochemistry*, *133*(3), 347–364. https://doi.org/10.1007/s10533-017-0338-5

Bowen, J. C., Ward, C. P., Kling, G. W., & Cory, R. M. (2020). Arctic amplification of global warming strengthened by sunlight oxidation of permafrost carbon to CO_2. *Geophysical Research Letters*, *47*(12), 1–8. https://doi.org/10.1029/2020GL087085

Bröder, L., Davydova, A., Davydov, S., Zimov, N., Haghipour, N., Eglinton, T. I., & Vonk, J. E. (2020). Particulate organic matter dynamics in a permafrost headwater stream and the Kolyma River mainstem. *Journal of Geophysical Research: Biogeosciences*, *125*(2), e2019JG005511. https://doi.org/10.1029/2019JG005511

Brothers, S., Bowes, D., Pearse, W. D., Tank, S. E., Vanengen, R., & Sibley, P. (2021). Declining summertime pCO_2 in tundra lakes in a granitic landscape. *Global Biogeochemical Cycles*, *35*(2), e2020GB006850. https://doi.org/10.1029/2020GB006850

Brown, Z. W., Lowry, K. E., Palmer, M. A., van Dijken, G. L., Mills, M. M., Pickart, R. S., & Arrigo, K. R. (2015). Characterizing the subsurface chlorphyll a maximum in the Chukchi Sea and Canada Basin. *Deep-Sea Research II*, *118*, 88–104. https://doi.org/10.1016/j.dsr2.2015.02.010

Burrows, R. M., Jonsson, M., Fältström, E., Andersson, J., & Sponseller, R. A. (2021). Interactive effects of light and nutrients on stream algal growth modified by forest management in boreal landscapes. *Forest Ecology and Management*, *492*, 119–212. https://doi.org/10.1016/j.foreco.2021.119212

Canning, A., Körtzinger, A., Fietzek, P., & Rehder, G. (2021). Technical note: Seamless gas measurements across Land-Ocean Aquatic Continuum - Corrections and evaluation of sensor data for CO_2, CH_4 and O_2 from field deployments in contrasting environments. *Biogeosciences*, *18*(4), 1351–1373. https://doi.org/10.5194/bg-18-1351-2021

Castro-Morales, K. (2025). Data presented in manuscript "Aquatic productivity signals in the Kolyma River (northeastern Siberia) from O_2/Ar ratios and O_2 triple isotopologues" by Castro-Morales et al. (Version 1.0) [Dataset]. *Zenodo*. https://doi.org/10.5281/zenodo.15229557

Castro-Morales, K., Canning, A., Arzberger, S., Overholt, W. A., Küsel, K., Kolle, O., et al. (2022). Highest methane concentrations in an Arctic river linked to local terrestrial inputs. *Biogeosciences*, *19*(21), 5059–5077. https://doi.org/10.5194/bg-19-5059-2022

Castro-Morales, K., Canning, A., Körtzinger, A., Göckede, M., Küsel, K., Overholt, W. A., et al. (2022). Effects of reversal of water flow in an Arctic stream on fluvial emissions of CO_2 and CH_4. *Journal of Geophysical Research: Biogeosciences*, *127*(1), e2021JG006485. https://doi.org/10.1029/2021JG006485

Castro-Morales, K., Cassar, N., Shoosmith, D. R., & Kaiser, J. (2013). Biological production in the Bellingshausen Sea from oxygen-to-argon ratios and oxygen triple isotopes. *Biogeosciences*, *10*(4), 2273–2291. https://doi.org/10.5194/bg-10-2273-2013

Catalán, N., Marcé, R., Kothawala, D. N., & Tranvik, L. J. (2016). Organic carbon decomposition rates controlled by water retention time across inland waters. *Nature Geoscience*, *9*, 501–506. https://doi.org/10.1038/NGEO2720

Clark, J. B., Mannino, A., Spencer, R. G. M., Tank, S. E., & McClelland, J. W. (2023). Quantification of discharge-specific effects on dissolved organic matter export from major Arctic Rivers from 1982 through 2019. *Global Biogeochemical Cycles*, *37*(8), e2023BG007854. https://doi.org/10.1029/2023GB007854

Codispoti, L. A., Kelly, V., Thessen, A., Matrai, P., Suttles, S., Hill, V., et al. (2013). Synthesis of primary production in the Arctic Ocean: III. Nitrate and phosphate based estimates of net community production. *Progress in Oceanography*, *110*, 126–150. https://doi.org/10.1016/j.pocean.2012.11.006

Collins, E. L., David, C. E., Riggs, R., Allen, G. H., Pavelsky, T. M., Lin, P., et al. (2024). Global patterns in river water storage dependent on residence time. *Nature Geoscience*, *17*(5), 433–439. https://doi.org/10.1038/s41561-024-01421-5

Cory, R. M., Ward, C. P., Crump, B. C., & Kling, G. W. (2014). Sunlight controls water column processing of carbon in arctic fresh waters. *Science*, *345*(6199), 925–928. https://doi.org/10.1126/science.1253119

Costard, F., Langer, M., Dumont, M., & Allard, M. (2007). Impact of climate change on permafrost and consequences on hydrology. *Permafrost and Periglacial Processes*, *18*(3), 271–275. https://doi.org/10.1002/ppp.595

Craig, H., & Hayward, T. (1987). Oxygen supersaturation in the ocean: Biological versus physical contributions. *Science*, *235*(4785), 202–205. https://doi.org/10.1126/science.235.4785.199

Crump, B. C., Peterson, B. J., Raymond, P. A., Amon, R. M. W., Rinehart, A., McClelland, J. W., & Holmes, R. M. (2009). Circumpolar synchrony in big river bacterioplankton. *Proceedings of the National Academy of Sciences of the United States of America*, *106*(50), 21208–21212. https://doi.org/10.1073/pnas.0906149106

Cullen, J. J. (2015). Maximum layers: Enduring enigma or mystery solved? *Annual Review of Marine Science*, *7*(1), 207–239. https://doi.org/10.1146/annurev-marine-010213-135111

Dean, J. F., Meisel, O. H., Martyn, R. M., Belelli, L. M., Garnett, M. H., Lenderink, H., et al. (2020). East Siberian Arctic inland waters emit mostly contemporary carbon. *Nature Communications*, *11*(1), 1627. https://doi.org/10.1038/s41467-020-15511-6

Descy, J.-P., Darchambeau, F., Lambert, T., Stoyneva-Gaertner, M. P., Bouillon, S., & Borges, A. V. (2017). Phytoplankton dynamics in the Congo River. *Freshwater Biology*, *62*(1), 87–101. https://doi.org/10.1111/fwb.12851

Dlugokencky, E. (2019). NOAA/GML. Retrieved from www.esrl.noaa.gov/gmd/ccgg/trends_ch4/

DOE. (1994). *Hand book of methods for the analysis of the various parameters of the carbon dioxide system in seawater, version 2*. Oak Ridge National Laboratory. https://doi.org/10.2172/10107773

Dokulil, M. T. (2015). Phytoplankton of the River Danube: Composition, seasonality and long-term dynamics. In I. Liska (Ed.), *The Danube River Basin*. Springeer-Verlag Berlin Heidelberg. https://doi.org/10.1007/698_2014_293

Dokulil, M. T., & Qian, K. (2021). Photosynthesis, carbon acquisition and primary productivity of phytoplankton: A review dedicated to Colin Reynolds. *Hydrobiologia*, *848*(1), 77–94. https://doi.org/10.1007/s10750-020-04321-y

Downing, B. D., Pellerin, B. A., Bergamaschi, B. A., Saraceno, J. F., & Kraus, T. E. C. (2012). Seeing the light: The effects of particles, dissolved materials, and temperature on in situ measurements of DOM fluorescence in rivers and streams. *Limnology and Oceanography: Methods*, *10*, 767–775. https://doi.org/10.4319/lom.2012.10.767

Emerson, S., Quay, P. D., Stump, C., Wilbur, D., & Schudlich, R. (1995). Chemical tracers of productivity and respiration in the subtropical Pacific Ocean. *Journal of Geophysical Research*, *100*(C8), 15873–15887. https://doi.org/10.1029/95JC01333

Eisenstadt, D., Barkan, E., Luz, B., & Kaplan, A. (2010). Enrichment of oxygen heavy isotopes during photosynthesis in phytoplankton. *Photosynthesis Research*, *103*(2), 97–103. https://doi.org/10.1007/s11120-009-9518-z

Engel, F., Attermeyer, K., Ayala, A. I., Fischer, H., Kirschesch, V., Pierson, D. C., & Weihenmeyer, G. A. (2019). Phytoplankton gross primary production increases along cascading impoundments in a temperate, low-discharge river: Insights from high frequency water quality monitoring. *Scientific Reports*, *9*(6701), 1–13. https://doi.org/10.1038/s41598-019-43008-w

Eveleth, R., Timmermans, M.-L., & Cassar, N. (2014). Physical and biological controls on oxygen saturation variability in the upper Arctic Ocean. *Journal of Geophysical Research: Oceans*, *119*(11), 7420–7432. https://doi.org/10.1002/2014JC009816

Fouilland, E., Gosselin, M., Rivkin, R. B., Vasseur, C., & Mostajir, B. (2007). Nitrogen uptake by heterotrophic bacteria and phytoplankton in Arctic surface waters. *Journal of Plankton Research*, *29*(4), 369–376. https://doi.org/10.1093/plankt/fbm022

Francis, A., Ganeshram, R. S., Tuerena, R. E., Spencer, R. G. M., Holmes, R. M., Rogers, J. A., & Mahaffey, C. (2023). Permafrost degradation and nitrogen cycling in Arctic rivers: Insights from stable nitrogen isotope studies. *Biogeosciences*, *20*(2), 365–382. https://doi.org/10.5194/bg-20-365-2023

Frey, K. E., & McClelland, J. (2009). Impacts of perfmafrost degradation on Arctic river biogeochemistry. *Hydrological Processes*, *23*(1), 169–182. https://doi.org/10.1002/hyp.7196

Fritz, M., Vonk, J. E., & Lantuit, H. (2017). Collapsing Arctic coastlines. *Nature Climate Change*, *7*(1), 6–7. https://doi.org/10.1038/nclimate3188

Gabyshev, V. A., & Gabysheva, O. I. (2013). The structure of phytoplankton and physicochemical characteristics of the Kolyma River (Northeastern Siberia) in summer. *Contemporary Problems of Ecology*, *6*(3), 268–275. https://doi.org/10.1134/s1995425513030074

García, H. E., & Gordon, L. I. (1992). Oxygen solubility in seawater: Better fitting equations. *Limnology & Oceanography*, *37*(6), 1307–1312. https://doi.org/10.4319/lo.1992.37.6.1307

Hamme, R. C., & Emerson, S. R. (2004). The solubility of neon, nitrogen and argon in distilled water and seawater. *Deep-Sea Research Part I Oceanographic Research Papers*, *51*(11), 1517–1528. https://doi.org/10.1016/j.dsr.2004.06.009

Hendricks, M. B., Bender, M. L., Barnett, B. A., Strutton, P., & Chavez, F. P. (2005). Triple oxygen isotope composition of dissolved O2 in the equatorial Pacific: A tracer of mixing, production and respiration. *Journal of Geophysical Research*, *110*(C12), C12021. https://doi.org/10.1029/2004jc002735

Hobbie, J. E., Peterson, B. J., Bettez, N., Deegan, L., O'Brien, W. J., Kling, G. W., et al. (1999). Impact of global change on the biogeochemistry and ecology of an Arctic freshwater system. *Special Issue: Proceedings of the International Symposium on Polar Aspects of Global Change*, *18*(2), 207–214. https://doi.org/10.3402/polar.v18i2.6576

Holger, C. (1997). *Die Dieatomeen der Laptevsee (Arktischer Ozean): Taxonomie, biogeographische Verbreitung und ozeanographische Bedeutung* (p. 98). Christian Albrechts University.

Holmes, R. M., McClelland, J. W., Peterson, B. J., Tank, S. E., Bulygina, E., Eglinton, T. I., et al. (2012). Seasonal and annual fluxes of nutrients and organic matter from large rivers to the Arctic Ocean and surrounding seas. *Estuaries and Coasts*, *35*(2), 369–382. https://doi.org/10.1007/s12237-011-9386-6

Holmes, R. M., Shiklomanov, A. I., Suslova, A., Tretiakov, M., McClelland, J. W., Scott, L., et al. (2021a). River discharge. 21-11. https://doi.org/10.25923/zevf-ar65

Holmes, R. M., Shiklomanov, A. I., Suslova, A., Tretiakov, M., McClelland, J. W., Scott, L., et al. (2021b). River discharge. *Bulletin of the American Meteorological Society*, S290–S292. https://doi.org/10.1175/BAMS-D-21-0086.1

Hotchkiss, E. R., Hall, R. O., Sponseller, R. A., Butman, D., Klaminder, J., Laudon, H., et al. (2015). Sources of and processes controlling CO_2 emissions change with the size of streams and rivers. *Nature Geoscience*, *8*(9), 696–699. https://doi.org/10.1038/ngeo2507

Hurry, V., Druart, N., Cavaco, A., Gardeström, P., & Strand, Å. (2002). Photosynthesis at low temperatures, A case study with Arabidopsis. In P. S. Li & E. T. Palva (Eds.), *Plant cold hardiness* (pp. 161–179). Springer. https://doi.org/10.1007/978-1-4615-0711-6_12

Huryn, A. D., Benstead, J. P., & Parker, S. M. (2014). Seasonal changes in light availability modify the temperature dependence of ecosystem metabolism in an arctic stream. *Ecology*, *95*(10), 2826–2839. https://doi.org/10.1002/ecy.2690

Ielpi, A., Lapôtre, M. G. A., Finotello, A., & Roy-Léveillée, P. (2023). Large Sinous rivers are slowing down in a warming Arctic. *Nature Climate Change*, *13*, 375–381. https://doi.org/10.1038/s41558-023-01620-9

Jones, A. E., Hodges, B. R., McClelland, J. W., Hardison, A. K., & Moffett, K. B. (2017). Residence-time-based classification of surface water systems. *Water Resources Research*, *53*(7), 5567–5584. https://doi.org/10.1002/2016WR019928

Juranek, L. W., & Quay, P. D. (2013). Using triple isotopes of dissolved oxygen to evaluate global marine productivity. *Annual Review of Marine Science*, *5*(1), 503-254. https://doi.org/10.1146/annurev-marine-121211-172430

Kaiser, J. (2011a). Technical note: Consistent calculation of aquatic gross production from oxygen triple isotope measurements. *Biogeosciences*, *8*(7), 1793–1811. https://doi.org/10.5194/bg-8-1793-2011

Kaiser, J. (2011b). Corrigendum to: "Technical note: Consistent calculation of aquatic gross production from oxygen triple isotope measurements" published in Biogeosciences, 8, 1973-1811, 2011. *Biogeosciences*, *8*(9), 2561–2565. https://doi.org/10.5194/bg-8-2561-2011

Kaiser, J., & Abe, O. (2012). Reply to Nicholson's comment on "Consistent calculation of aquatic gross production from oxygen triple isotope measurements" by Kaiser (2011). *Biogeosciences*, *9*(8), 2921–2933. https://doi.org/10.5194/bg-9-2921-2012

Kaiser, J., Reuer, M. K., Barnett, B., & Bender, M. L. (2005). Marine productivity estimates from continuous O_2/Ar ratio measurements by membrane inlet mass spectrometry. *Geophysical Research Letters*, *32*(19), L19605. https://doi.org/10.1029/2005GL023459

Keskitalo, K. H., Bröder, L., Jong, D. J., Zimov, N., Davydova, A., Davydov, S., et al. (2022). Seasonal variability in particulate organic carbon degradation in the Kolyma River, Siberia. *Environmental Research Letters*, *17*(3), 034007. https://doi.org/10.1088/1748-9326/ac4f8d

King, T. V., Neilson, B. T., Overbeck, L. D., & Kane, D. L. (2016). Water temperature controls in low arctic rivers. *Water Resources Research*, *52*(6), 4358–4376. https://doi.org/10.1002/2015WR017965

Kittler, F., Eugster, W., Foken, T., Heimann, M., Kolle, O., & Göckede, M. (2017). High-quality eddy-covariance CO_2 budgets under cold climate conditions. *Journal of Geophysical Research: Biogeosciences*, *122*(8), 2064–2084. https://doi.org/10.1002/2017JG003830

Knox, M., Quay, P. D., & Wilbur, D. (1992). Kinetic isotopic fractionation during air-water gas transfer of O_2, N_2, CH_4, and H_2. *Journal of Geophysical Research*, *97*(C12), 20335–20343. https://doi.org/10.1029/92jc00949

Koch, B. P., & Dittmar, T. (2006). From mass to structure: An aromaticity index for high-resolution mass data of natural organic matter. *Rapid Communications in Mass Spectrometry*, *20*(5), 926–932. https://doi.org/10.1002/rcm.7433

Kügler, S., Cooper, R. E., Wegner, C.-E., Mohr, J. F., Wichard, T., & Küsel, K. (2019). Iron-organic matter complexes accelerate microbial iron cycling in an iron-rich fen. *Science of the Total Environment*, *646*, 972–988. https://doi.org/10.1016/j.scitotenv.2018.07.258

Lewis, E. L., Wallace, D. W. R., & Allison, L. J. (1998). *Program developed for CO2 system calculations*. Brookhaven National Lab., Department of Applied Science and Oak Ridge National Lab., Carbon Dioxide Information Analysis Center. https://doi.org/10.2172/639712

Li, Y.-H., & Peng, T.-H. (2002). Latitudinal change of remineralization ratios in the oceans and its implication for nutrient cycles. *Global Biogeochemical Cycles*, *16*(4), 1130. https://doi.org/10.1029/2001GB001828

Listwan, S., Tokarek, W., Kleszcz, K., Chowaniec, M., Porębska, Z., Krawczyk, K., et al. (2018). Phaeodactlum tricornutum as potential phytoremediator of sea and fresh waters. Paper presented at Proceedings of the 4th world congress on new technologies (New Tech'18), Madrid, Spain.

Liu, S., & Raymond, P. A. (2018). Hydrologic controls on pCO_2 and CO_2 efflux in US streams and rivers. *Limnology and Oceanography Letters*, *3*(6), 428–435. https://doi.org/10.1002/lol2.10095

Luz, B., & Barkan, E. (2000). Assessment of oceanic productivity with the triple-isotope composition of dissolved oxygen. *Science*, *288*(5473), 2028–2031. https://doi.org/10.1126/science.288.5473.2028

Luz, B., & Barkan, E. (2005). The isotopic ratios $^{17}O/^{16}O$ and $^{18}O/^{16}O$ in molecular oxygen and their significance in biogeochemistry. *Geochimica et Cosmochimica Acta*, *69*(5), 1099–1110. https://doi.org/10.1016/j.gca.2004.09.001

Luz, B., & Barkan, E. (2009). Net and gross oxygen production from O_2/Ar, $^{17}O/^{16}O$ and $^{18}O/^{16}O$ ratios. *Aquatic Microbial Ecology*, *56*, 133–145. https://doi.org/10.3354/ame01296

Luz, B., & Barkan, E. (2010). Variations of $^{17}O/^{16}O$ and $^{18}O/^{16}O$ in meteoric waters. *Geochimica et Cosmochimica Acta*, *74*(22), 6276–6286. https://doi.org/10.1016/j.gca.2010.08.016

Luz, B., Barkan, E., Bender, M. L., Thiemens, M. H., & Boering, K. A. (1999). Triple-isotope composition of atmospheric oxygen as a tracer of biospehre productivity. *Nature*, *400*(6744), 547–550. https://doi.org/10.1038/22987

Luz, B., Barkan, E., Sagi, Y., & Yacobi, Y. Z. (2002). Evaluation of community respiratory mechanisms with oxygen isotopes: A case study in Lake Kinneret. *Limnology & Oceanography*, *47*(1), 33–42. https://doi.org/10.4319/lo.2002.47.1.0033

Ma, Y., Mao, R., & Li, S. (2021). Hydrological seasonality largely contributes to riverine dissolved organic matter chemical composition: Insights from EEM-PARAFAC and optical indicators. *Journal of Hydrology*, *595*, 125993. https://doi.org/10.1016/j.jhydrol.2021.125993

Mackay, E. B., Feuchtmayr, H., De Ville, M. M., Thackeray, S. J., Callaghan, N., Marshall, M., et al. (2020). Dissolved organic nutrient uptake by riverine phytoplankton varies along a gradient of nutrient enrichment. *Science of the Total Environment*, *722*, 137837. https://doi.org/10.1016/j.scitotenv.2020.137837

Makarieva, O., Shikhov, A., Ostashov, A., & Nesterova, N. (2020). Aufeis (nadels) of the North-East of Russia: GIS catalogue for the Kolyma River basin [Dataset]. *PANGAEA*. https://doi.org/10.1594/PAGAEA.925406

Mann, P. J., Davydova, A., Zimov, N., Spencer, R. G. M., Davydov, S., Bulygina, E., et al. (2012). Controls on the composition and lability of dissolved organic matter in Siberia's Kolyma River basin. *Journal of Geophysical Research*, *117*(G1), G01028. https://doi.org/10.1029/2011JG001798

Mann, P. J., Eglinton, T. I., McIntyre, C. P., Zimov, N., Davydova, A., Vonk, J. E., et al. (2015). Utilization of ancient permafrost carbon in headwaters of Arctic fluvial networks. *Nature Communications*, *6*(7856), 1–7. https://doi.org/10.1038/ncomms8856

Matrai, P. A., Olson, E., Suttles, S., Hill, V., Codispoti, L. A., Light, B., & Steele, M. (2013). Synthesis of primary production in the Arctic Ocean: I. Surface waters, 1954-2007. *Progress in Oceanography*, *110*, 93–106. https://doi.org/10.1016/j.pocean.2012.11.004

McClelland, J. W., Holmes, R. M., Peterson, B. J., & Stieglitz, M. (2004). Increasing river discharge in the Eurasian Arctic: Consideration of dams, permafrost thaw, and fires as potential agents of change. *Journal of Geophysical Research*, *109*(D18), D18102. https://doi.org/10.1029/2004JD004583

Meredith, M., Sommerkorn, M., Cassotta, S., Derksen, C., Ekaykin, A., Hollowed, A., et al. (2019). Polar regions. 203–320. https://doi.org/10.1017/9781009157964.005

Miller, N. A. (2013). *Changes in net ecosystem production over the past 40 years in Arctic tundra pondes near Barrow, Alaska: Application of historic and modern techniques*. University of Texas at El Paso.

Millero, F. J. (1979). The thermodynamics of the carbonate system in seawater. *Geochimica et Cosmochimica Acta*, *43*(10), 1651–1661. https://doi.org/10.1016/0016-7037(79)90184-4

Myrstener, M., Fork, M. L., Bergström, A.-K., Castillo Puts, I., Hauptmann, D., Isles, P. D. F., et al. (2022). Resolving the drivers of algal nutrient limitation from Boreal to Arctic Lakes and Streams. *Ecosystems*, *25*(8), 1682–1699. https://doi.org/10.1007/s10021-022-00759-4

Myrstener, M., Rocher-Ros, G., Burrows, R. M., Bergström, A.-K., Giesler, R., & Sponseller, R. A. (2018). Persisten nitrogen limitation of stream biofilm communities along climate gradients in the Arctic. *Global Change Biology*, *24*(8), 3680–3691. https://doi.org/10.1111/gcb.14117

O'Donnell, J. A., Aiken, G. R., Swanson, D. K., Panda, S., Butler, K. D., & Baltensperger, A. P. (2016). Dissolved organic matter composition of Arctic rivers: Linking permafrost and parent material to riverine carbon. *Global Biogeochemical Cycles*, *30*(12), 1811–1826. https://doi.org/10.1002/2016GB005482

O'Donnell, J. A., Carey, M. P., Koch, J. C., Baughman, C., Hill, K., Zimmerman, C. E., et al. (2024). Metal mobilization from thawing permafrost to aquatic ecosystems is driving rusting of Arctic streams. *Communications Earth & Environment*, *5*(268), 1–10.

Oliver, B. G., Thurman, E. M., & Malcom, R. L. (1983). The contribution of humic substances to the acidity of colored natural waters. *Geochimica et Cosmochimica Acta*, *47*(11), 2031–2035. https://doi.org/10.1016/0016-7037(83)90218-1

Park, H., Ko, N.-Y., Kim, J., Opel, T., Meyer, H., Wetterich, S., et al. (2022). Composition and origins of greenhouse gas species in permafrost ice wedges at the Batagay megaslump, Yana Uplands, Northeast Siberia. In E. G. Union (Ed.), *EGU General Assembly 2022*. https://doi.org/10.5194/egusphere-egu22-3437

Potapova, M. (2014). Diatoms of bering Island, Kamchatka, Russia. *Nova Hedwigia*, *143*, 63–102. https://doi.org/10.1127/1438-9134/2014/004

Potapova, M. (2019). Retrieved from https://diatoms.org/species/melosira_varians

Pratiwi, H., Damar, A., & Sulistiono, S. (2018). Phytoplankton community structure in the estuary of Donan River, Cilacap, Central Java, Indonesia. *Biodiversitas Journal of Biological Diversity*, *19*(6), 2104–2110. https://doi.org/10.13057/biodiv/d190616

Quay, P. D., Peacock, C., Björkman, K., & Karl, D. M. (2010). Measuring primary production rates in the ocean: Enigmatic results between incubation and non-incubation methods at station ALOHA. *Global Biogeochemical Cycles*, *24*, GB3014. https://doi.org/10.1029/2009GB003665

Rantanen, M., Karpechko, A. Y., Lipponen, A., Nordling, K., Hyvärinen, O., Ruosteenoja, K., et al. (2022). The Arctic has warmed nearly four times faster than the globe since 1979. *Communications Earth & Environment*, *3*(168), 1–10. https://doi.org/10.1038/s43247-022-00498-3

Raymond, P. A., Hartmann, J., Lauerwald, R., Sobek, S., McDonald, C., Hoover, M., et al. (2013). Global carbon dioxide emissions from inland waters. *Nature*, *503*(7476), 355–359. https://doi.org/10.1038/nature12760

Raymond, P. A., Zappa, C. J., Butman, D., Bott, T. L., Potter, J. D., Mulholland, P., et al. (2012). Scaling the gas transfer velocity and hydraulic geometry in streams and small rivers. *Limnology and Oceanography: Fluids and Environments*, *2*(1), 41–53. https://doi.org/10.1215/21573689-1597669

Regaudie-de-Gioux, A., Lasternas, S., Agustí, S., & Duarte, C. M. (2014). Comparing marine primary production estimates through different methods and development of conversion equations. *Frontiers in Marine Science*, *1*(19). https://doi.org/10.3389/fmars.2014.00019

Rocher-Ros, G., Harms, T. K., Sponseller, R. A., Väisänen, M., Mörth, C.-M., & Giesler, R. (2020). Metabolism overrides photo-oxidation in CO_2 dynamics of Arctic permafrost streams. *Limnology & Oceanography*, 1–13. https://doi.org/10.1002/lno.11564

Rocher-Ros, G., Sponseller, R. A., Bergström, A.-K., Myrstener, M., & Giesler, R. (2019). Stream metabolism controls diel patterns and evasion of CO_2 in Arctic streams. *Global Change Biology*, *26*(3), 1400–1413. https://doi.org/10.1111/gcb.14895

Rollo, C., Heywood, K. J., Hall, R. A., Barton, E. D., & Kaiser, J. (2020). Glider observations of the Northwestern Iberian Margin during an exceptional summer upwelling season. *Journal of Geophysical Research*, *125*(8), e2019JC015804. https://doi.org/10.1029/2019JC015804

Röst, H. L., Sachsenberg, T., Aiche, S., Bielow, C., Weisser, H., Aicheler, F., et al. (2016). OpenMS: A flexible open-source software platform for mass spectrometry data analysis. *Nature Methods*, *13*(9), 741–748. https://doi.org/10.1038/nmeth.3959

Rovelli, L., Olde, L. A., Heppell, C. M., Binley, A., Yvon-Durocher, G., Glud, R. N., & Trimmer, M. (2022). Contrasting biophysical controls on carbon dioxide and methane outgassing from streams. *Journal of Geophysical Research: Biogeosciences*, *127*(1), e2021JG006328. https://doi.org/10.1029/2021JG006328

Schmid, M., & Read, J. (2022). Heat budget of lakes. In T. Mehner & K. Tockner (Eds.), *Encyclopedia of inland waters* (2nd ed., pp. 467–473). Elsevier. https://doi.org/10.1016/B978-0-12-819166-8.00011-6

Schmidt, A. (1988). Sulfur metabolism in Cyanobacteria. *Methods in Enzymology*, *167*, 572–583. https://doi.org/10.1016/0076-6879(88)67065-0

Schulz, G., van Beusekom, J. E. E., Jacob, J., Bold, S., Schöl, A., Ankele, M., et al. (2023). Low discharge intensifies nitrogen retention in rivers - A case study in the Elbe River. *Science of the Total Environment*, *904*, 166740. https://doi.org/10.1016/j.scitotenv.2023.166740

Schuur, E. A., McGuire, D., Schädel, C., Grosse, G., Harden, J. W., Hayes, D. J., et al. (2015). Climate change and the permafrost carbon feedback. *Nature*, *520*(7546), 171–179. https://doi.org/10.1038/nature14338

Schuur, E. A. G., Abbott, B. W., Commane, R., Ernakovich, J., Euskirchen, E., Hugelius, G., et al. (2022). Permafrost and Climate Change: Carbon cycle feedbacks from the warming Arctic. *Annual Review of Environment and Resources*, *47*(1), 343–371. https://doi.org/10.1146/annurev-environ-012220-011847

Seguro, I., Marca, A. D., Shutler, J. D., & Kaiser, J. (2023). Different flavours of oxygen help quantify seasonal variations of the biological carbon pump in the Celtic Sea. *Frontiers in Marine Science*, *10*, 1037470. https://doi.org/10.3389/fmars.2023.1037470

Seguro, I., Marca, A. D., Suzanne, J. P., Shutler, J. D., Suggett, D. J., & Kaiser, J. (2017). High-resolution net and gross biological production during a Celtic Sea spring bloom. *Progress in Oceanography*, *177*, 101885. https://doi.org/10.1016/j.pocean.2017.12.0003

Serikova, S., Pokrovsky, O. S., Ala-Aho, P., Kazantsev, V., Kirpotin, S. N., Kopysov, S. G., et al. (2018). High riverine CO2 emissions at the permafrost boundary of Western Siberia. *Nature Geoscience*, *11*, 825–829. https://doi.org/10.1038/s41561-018-0218-1

Shiklomanov, A. I., Holmes, R. M., McClelland, J. W., Tank, S. E., & Spencer, R. G. M. (2020). Discharge Dataset (20200713) [Dataset]. Retrieved from https://arcticgreatrivers.org/water_data/

Snyder, L., Potter, J. D., & McDowell, W. H. (2018). An evaluation of nitrate, fDOM, and turbidity sensors in New Hampshire Streams. *Water Resources Research*, *54*(3), 2466–2479. https://doi.org/10.1002/2017WR020678

Sorokin, Y. I., & Sorokin, P. Y. (1996). Plankton and Primary production in the Lena River estuary and in the South-eastern Laptev Sea. *Estuarine, Coastal and Shelf Science*, *43*(4), 399–418. https://doi.org/10.1006/ecss.1996.0078

Spencer, R. G. M., Aiken, G. R., Wickland, K. P., Striegl, R., & Hernes, P. J. (2008). Seasonal and spatial variability in dissolved organic matter quantity and composition from the Yukon River basin, Alaska. *Global Biogeochemical Cycles*, *22*(4), GB4002. https://doi.org/10.1029/2008GB003231

Spencer, R. G. M., Mann, P. J., Dittmar, T., Eglinton, T. I., McIntyre, C. P., Holmes, R. M., et al. (2015). Detecting the signature of permafrost thaw in Arctic rivers. *Geophysical Research Letters*, *42*(8), 2830–2835. https://doi.org/10.1002/2015GL063498

Squires, M. M., Lesack, L. F. W., Hecky, R. E., Guildford, S. J., Ramlal, P., & Higgins, S. N. (2009). Primary production and carbon dioxide metabolic balance of a lake rich Arctic river floodplain: Partitioning of phytoplankton epipelon, macrophyte, and epiphyton production among lakes on the Mackenzie Delta. *Ecosystems*, *12*(5), 853–872. https://doi.org/10.1007/s10021-009-9263-3

Stanley, R. H. R., Kirkpatrick, J. B., Cassar, N., Barnett, B. A., & Bender, M. L. (2010). Net community production and gross primary production rates in the western equatorial Pacific. *Global Biogeochemical Cycles*, *24*(4), GB4001. https://doi.org/10.1029/2009GB003651

Stanley, R. H. R., Sandwith, Z. O., & Williams, W. J. (2015). Rates of summertime biological productivity in the Beaufort Gyre: A comparison between the low and record-low ice conditions of August 2011 and 2012. *Journal of Marine Systems*, *147*, 29–44. https://doi.org/10.1016/j.jmarsys.2014.04.006

Stubbins, A., Mann, P. J., Powers, L., Bittar, T. B., Dittmar, T., McIntyre, C. P., et al. (2017). Low photolability of yedoma permafrost dissolved organic carbon. *Journal of Geophysical Research: Biogeosciences*, *122*(1), 200–211. https://doi.org/10.1002/2016JG003688

Suryaningtyas, I. T., Permadi, S., Solikin, Jasmadi, Sapulete, S., Suparmo, & Widyartini, D. S. (2022). Growth and lipid profiles of *Melosira sp.* in response to different salinity levels. *Journal of Aquaculture and Fish Health*, *11*(2), 216–226. https://doi.org/10.20473/jafh.v11i2.30388

Sutherland, K. M., Johnston, D. T., Hemingway, J. D., Wankel, S. D., & Ward, C. P. (2022). Revised microbial and photochemical triple-oxygen isotope effects improve marine gross oxygen production estimates. *Proceedings of the Academy of Natural Sciences Nexus*, *1*(5), pgac233. https://doi.org/10.1093/pnasnexus/pgac233

Teeter, L., Hamme, R. C., Ianson, D., & Bianucci, L. (2018). Accurate estimation of net community production from O_2/Ar measurements. *Global Biogeochemical Cycles*, *32*(8), 1163–1181. https://doi.org/10.1029/2017GB005874

Terhaar, J., Lauerwald, R., Regnier, P. A. G., Gruber, N., & Bopp, L. (2021). Around one third of current Arctic Ocean primary production sustained by rivers and coastal erosion. *Nature Communications*, *12*(169), 1–10. https://doi.org/10.1038/s41467-020-20470-z

Turetsky, M. R., Abbott, B. W., Jones, M. C., Walter Anthony, K., Olefeldt, D., Schuur, E. A., et al. (2020). Carbon release through abrupt permafrost thaw. *Nature Geoscience*, *13*(2), 138–143. https://doi.org/10.1038/s41561-019-0526-0

Ulfsbo, A., Cassar, N., Korhonen, M., van Heuven, S., Hoppema, M., Kattner, G., & Anderson, L. G. (2014). Late summer net community production in the central Arctic Ocean using multiple approaches. *Global Biogeochemical Cycles*, *28*(10), 1129–1148. https://doi.org/10.1002/2014GB004833

Vishnivetskaya, T. A., Almatari, A. L., Spirina, E. V., Wu, X., Williams, D. E., Pfiffner, S. M., & Rivkina, E. M. (2020). Insights into community photosynthetic microorganisms from permafrost. *FEMS Microbiology Ecology*, *96*(12), fiaa229. https://doi.org/10.1093/femsec/fiaa229

Vonk, J. E., Tank, S. E., Bowden, W. B., Laurion, I., Vincent, W. F., Alekseychik, P., et al. (2015). Reviews and syntheses: Effects of permafrost thaw on Arctic aquatic ecosystems. *Biogeosciences*, *12*(23), 7129–7167. https://doi.org/10.5194/bg-12-7129-2015

Vonk, J. E., Tank, S. E., Mann, P. J., Spencer, R. G. M., Treat, C. C., Striegl, R. G., et al. (2015). Biodegradability of dissolved organic carbon in permafrost soils and aquatic systems: A meta-analysis. *Biogeosciences*, *12*(23), 6915–6930. https://doi.org/10.5194/bg-12-6915-2015

Wanninkhof, R. (1992). Relationship between gas exchange and wind speed over the ocean. *Journal of Geophysical Research*, *97*, 7373–7381. https://doi.org/10.1029/92JC00188

Wanninkhof, R. (2014). Relationship between wind speed and gas exchange over the ocean revisited. *Limnology and Oceanography: Methods*, *12*(6), 351–362. https://doi.org/10.4319/lom.2014.12.351

Ward, N. D., Bianchi, T. S., Medeiros, P. M., Seidel, M., Richey, J. E., Keil, R. G., & Sawakuchi, H. O. (2017). Where carbon goes when water flows: Carbon cycling across the Aquatic Continuum. *Frontiers in Marine Science*, *4*(7). https://doi.org/10.3389/fmars.2017.00007

Watras, C. J., Hanson, P. C., Stacy, T. L., Morrison, K. M., Mather, J., Hu, Y.-H., & Milewski, P. (2011). A temperature compensation method for CDOM fluorescence sensors in freshwater. *Limnology and Oceanography: Methods*, *9*(7), 296–301. https://doi.org/10.4319/lom.2011.9.296

Welp, L. R., Randerson, J. T., Finlay, J. C., Davydov, S. P., Zimova, G. M., Davydova, A. I., & Zimov, S. (2005). A high-resolution time series of oxygen isotopes from the Kolyma River: Implications for the seasonal dynamics of discharge and basin-scale water use. *Geophysical Research Letters*, *32*(L14401). https://doi.org/10.1029/2005GL022857

Wetterich, S., Nazarova, L. B., Larisa, B., Palagushkina, O. V., Syrykh, L. S., Savelieva, L. A., & Bobrov, A. A. (2017). Diatoms in sediment samples from the pingo exposure [Dataset]. https://doi.org/10.1594/PANGAEA.884365

Wetterich, S., Schirrmeister, L., Nazarova, L. B., Larisa, B., Palagushkina, O. V., Bobrov, A. A., et al. (2018). Holocene thermokarst and pingo development in the Kolyma Lowland (NE Siberia). *Permafrost and Periglacial Processes*, *29*(3), 182–198. https://doi.org/10.1002/ppp.1979

Wild, B., Andersson, A., Bröder, L., Vonk, J. E., Hugelius, G., McClelland, J. W., et al. (2019). Rivers across the Siberian Arctic unearth the patterns of carbon release from thawing permafrost. *Proceedings of the National Academy of Sciences of the United States of America*, *116*(21), 10280–10285. https://doi.org/10.1073/pnas.1811797116

Winterdahl, M., Wallin, M. B., Huseby Karlsen, R., Laudon, H., Öquist, M., & Lyon, S. W. (2016). Decoupling of carbon dioxide and dissolved organic carbon in boreal headwater streams. *Journal of Geophysical Research: Biogeosciences*, *121*(10), 2630–2651. https://doi.org/10.1002/2016JG003420

Wrona, F. J., Prowse, T. D., Reist, J. D., Hobbie, J. E., Lévesque, L. M. J., & Vincent, W. F. (2006). Climate change effects on aquatic biota, ecosystem structure and function. *Ambio*, *35*(7), 359–369. https://doi.org/10.1579/0044-7447(2006)35[359:cceoab]2.0.co;2

Yang, C., Yang, P., Geng, J., Yin, H., & Chen, K. (2020). Sediment internal nutrient loading in the most polluted area of a shallow eutrophic lake (Lake Chaohu, China) and its contribution to lake eutrophication. *Environmental Pollution*, *262*, 114292. https://doi.org/10.1016/j.envpol.2020.114292

Yun, M. S., Whitledge, T. E., Stockwell, D., Son, S. H., Lee, J. H., Park, J. W., et al. (2016). Primary production in the Chuckchi Sea with potential effects of freshwater content. *Biogeosciences*, *13*(3), 737–749. https://doi.org/10.5194/bg-13-737-2016

Zhang, Y., van Dijk, M. A., Liu, M., Zhu, G., & Qin, B. (2009). The contribution of phytoplankton degradation to chromophoric dissolved organic matter (CDOM) in eutrophic shallow lakes: Field and experimental evidence. *Water Research*, *43*(18), 4685–4697. https://doi.org/10.1016/j.watres.2009.07.024

References From the Supporting Information

Alsufyani, T., Weiss, A., & Wichard, T. (2017). Time course exo-metabolomic profiling in the green marine macroalga Ulva (Chlorophyta) for identification of growth phase-dependent biomarkers. *Marine Drugs*, *15*(1), 14. https://doi.org/10.3390/md15010014

Anderson, M., & Willis, T. (2003). Canonical analysis of principal coordinates: A useful method of constrained ordination for ecology. *Ecology*, *84*(2), 511–525. https://doi.org/10.1890/0012-9658(2003)084[0511:CAOPCA]2.0.CO;2

Anderson, M. J., & Robinson, J. (2003). Generalized discriminant analysis based on distances. *Australian & New Zealand Journal of Statistics*, *45*(3), 301–318. https://doi.org/10.1111/1467-842X.00285

Becker, S., Aoyama, M., Malcom, E., Woodward, S., Bakker, K., Coverly, S., et al. (2019). GO-SHIP Repeat Hydrography Nutrient Manual: The precise and accurate determination of dissolved inorganic nutrients in seawater, using Continuous Flow Analysis methods. 55. https://doi.org/10.25607/OBP-555

Callahan, B. J., McMurdie, P. J., Rosen, M. J., Han, A. W., Johnson, A. J. A., & Holmes, S. P. (2016). DADA2: High-resolution sample interference from Illumina amplicon data. *Nature Methods*, *13*(7), 581–583. https://doi.org/10.1038/nmeth.3869

Djemiel, C., Plassard, D., Terrat, S., Crouzet, O., Sauze, J., Mondy, S., et al. (2020). µgreen-db: A reference database for the 23S rRNA gene of eukaryotic plastids and Cyanobacteria. *Scientific Reports*, *10*(1), 5915. https://doi.org/10.1038/s41598-020-62555-1

Fu, Q.-L., Fujii, M., & Riedel, T. (2020). Development and comparison of formula assignment algorithms for ultrahigh-resolution mass spectra of natural organic matter. *Analytica Chimica Acta*, *1125*, 247–257. https://doi.org/10.1016/j.aca.2020.05.048

Gehre, M., Geilmann, H., Richter, J., Werner, R. A., & Brand, W. A. (2004). Continuous flow 2H/1H and 18O/16O analysis of water samples with dual inlet precision. *Rapid Communications in Mass Spectrometry*, *18*(22), 2650–2660. https://doi.org/10.1002/rcm.1672

Koch, B. P., Dittmar, T., Witt, M., & Kattner, G. (2007). Fundamentals of molecular formula assignment to ultrahigh resolution mass data of natural organic matter. *Analytical Chemistry*, *79*(4), 1758–1763. https://doi.org/10.1021/ac061949s

Leefmann, T., Frickenhaus, S., & Koch, B. P. (2019). UltraMassExplorer: A browser-based application for the evaluation of high-resolution mass spectrometric data. *Rapid Communications in Mass Spectrometry*, *33*(2), 193–202. https://doi.org/10.1002/rcm.8315

Martin, M. (2011). Cutadapt removes adapter sequences from high-throughput sequencing reads. *EMBnet.journal*, *17*(1), 10. https://doi.org/10.14806/ej.17.1.200

Minor, E. C., Swenson, M. M., Mattson, B. M., & Oyler, A. R. (2014). Structural characterization of dissolved organic matter: A review of current techniques for isolation and analysis. *Environmental Sciences: Processes & Impacts*, *16*(9), 2064–2079. https://doi.org/10.1039/C4EM00062E

Oksanen, J., Kindt, R., Legendre, P., O'Hara, B., Stevens, M. H. H., Oksanen, M. J., & Suggests, M. A. S. S. (2007). The vegan package: Community ecology package. *R package version*.

Parada, A. E., Needham, D. M., & Fuhrman, J. A. (2016). Every base matters: Assessing small subunit rRNA primers for marine microbiomes with mock communities, time series and global field samples. *Environmental Microbiology*, *18*(5), 1403–1414. https://doi.org/10.1111/1462-2920.13023

Paulson, J. N., Stine, O. C., Bravo, H. C., & Pop, M. (2013). Differential abundance analysis for microbial marker-gene surveys. *Nature Methods*, *10*(12), 1200–1202. https://doi.org/10.1038/nmeth.2658

Quast, C., Pruesse, E., Yilmaz, P., Gerken, J., Schweer, T., Yarza, P., et al. (2012). The SILVA ribosomal RNA gene database project: Improved data processing and web-based tools. *Nucleic Acids Research*, *41*(D1), D590–D596. https://doi.org/10.1093/nar/gks1219

Quince, C., Lanzen, A., Davenport, R. J., & Turnbaugh, P. J. (2011). Removing noise from pyrosequenced amplicons. *BMC Bioinformatics*, *12*(1), 38. https://doi.org/10.1186/1471-2105-12-38

Shiklomanov, A. I., Holmes, R. M., McClelland, J. W., Tank, S. E., & Spencer, R. G. M. (2020). In A. G. R. Observatory (Ed.), *Discharge dataset*.

Van Krevelen, D. (1950). Graphical-statistical method for the study of structure and reaction processes of coal. *Fuel*, *29*, 269–284.

Wang, Z., Hoffmann, T., Six, J., Kaplan, J. O., Govers, G., Doetterl, S., & Van Oost, K. (2017). Human-induced erosion has offset one-third of carbon emissions from land cover change. *Nature Climate Change*, *7*(5), 345–350. https://doi.org/10.1038/nclimate3263

Wickham, H., François, R., Henry, L., & Müller, K. (2019). dplyr: A grammar of data manipulation. *R package version*.